UNIVERSITY OF CALIFORNIA,
IRVINE

Optical Control of Hierarchical Graphene Systems in Ultraviolet to Mid-infrared Region through Varying Surface Profiles and Nanoparticle Coatings

THESIS

submitted in partial satisfaction of the requirements
for the degree of

MASTER OF SCIENCE

in Chemical and Biomolecular Engineering

by

Yi Tuan

Thesis Committee:
Professor Vasan Venugopalan, Chair
Associate Professor Jaeho Lee
Professor Vojislav Stamenkovic

2021

DEDICATION

To

my family and friends

in recognition of their worth and unconditional support

Shoot for the moon. Even if you miss, you'll land among the stars.

Les Brown

TABLE OF CONTENTS

Page

LIST OF FIGURES iv

LIST OF TABLES vi

ACKNOWLEDGEMENTS vii

ABSTRACT OF THE THESIS viii

INTRODUCTION 1

CHAPTER 1: Biaxially-Strained Randomly Crumpled Graphene 5
- Sample Geometry and Computational Methods 5
- Optical Properties 6
  - Variation in Correlation Length (ξ) and Root-Mean-Square Amplitude (α) 6
  - Variation in Thickness (δ) 7

CHAPTER 2: Gold Particle-Coated Periodically Crumpled Graphene 9
- Sample Geometry and Computational Methods 9
- Optical Properties 10
  - Variation in Amplitude (A) and Pitch (P) 10
  - Variation in Particle Radius (r) 13
  - Variation in Particle Separation (λ) 15
- Optimization of Design 16

CHAPTER 3: Thermal Properties 18
- Biaxially-Strained Randomly Crumpled Graphene 18
- Gold Particle-Coated Periodically Crumpled Graphene 19

CHAPTER 4: Discussion 23

CHAPTER 5: Conclusion 24

REFERENCES 25

APPENDIX A: Supplementary 30

LIST OF FIGURES

Page

Figure 1 Schematic and simulation object in FDTD of biaxially-strained randomly crumpled graphene 5

Figure 2 Spectral average absorbance of biaxially-strained randomly crumpled graphene as a function of aspect ratio for three different fixed correlation lengths (ξ = 0.25, 0.75, 1.50 μm) obtained through FDTD simulations. 6

Figure 3 Reflectivity and absorbance of biaxially-strained randomly crumpled graphene in the near-infrared region with varying thickness (δ = 0.35, 1.05, 1.75, 3.5 nm) obtained through FDTD simulations 8

Figure 4 Schematic and simulation object in FDTD of gold particle-coated periodically crumpled graphene 10

Figure 5 Effect of changing amplitude (A) and pitch (P) on the structure and absorbance in the ultraviolet-near-infrared (UV-NIR, 0.05–1 μm) region of gold particle-coated periodically crumpled graphene 12

Figure 6 Reflectivity, transmittance, and absorbance of gold particle-coated periodically crumpled graphene in the mid-infrared (MIR) region with varying pitch (P = 0.14, 0.2, 0.4, 0.6, 0.8, 1 μm) and amplitude (A = 0.025, 0.05, 0.1, 0.2 μm) obtained through FDTD simulations 12

Figure 7 Reflectivity, transmittance, and absorbance of gold particle-coated periodically crumpled graphene in the ultraviolet-near-infrared (UV-NIR) region with varying gold particle radius (r = 4.1875 (R/4), 8.375 (R/2), 16.75 (R), 33.5 (2R), 67 nm (4R)) for two different pitch values (P = 0.4, 1 μm) obtained through FDTD simulations. Spectral average absorbance in the NIR as a function of particle radius for the two different pitch values. 14

Figure 8 Reflectivity, transmittance, and absorbance of gold particle-coated periodically crumpled graphene in the mid-infrared (MIR) region with varying particle radius (r = 4.1875 (R/4), 8.375 (R/2), 16.75 (R), 33.5 (2R), 67 nm (4R)) for two pitch values (P = 0.4, 1 μm) obtained through FDTD simulations 15

Figure 9 Reflectivity, transmittance, and absorbance of gold particle-coated periodically crumpled graphene in the ultraviolet-near-infrared to mid-infrared (UV-NIR to MIR) region with varying gold particle separation (λ = 0.05, 0.1, 0.2 μm) obtained through FDTD simulations. (c) Spectral average absorbance and transmittance in the UV-NIR as a function of particle separation 16

Figure 10 Plots of the cross-sectional electric field (V/m) in the x-z plane and corresponding solar absorbance indicate an optimal geometric configuration for maximal heating in gold particle-coated periodically crumpled graphene 17

Figure 11 Effect of correlation length (ξ), RMS amplitude (α), and (b) thickness on radiative cooling performance of biaxially-crumpled randomly crumpled graphene obtained through MATLAB 19

Figure 12 Effect of pitch (P) and (b) amplitude (A) on radiative cooling performance of gold particle-coated periodically crumpled graphene obtained through MATLAB 20

Figure 13 Effect of particle radius (r) and (c) particle separation (λ) on radiative cooling performance of gold particle-coated crumpled graphene obtained through MATLAB 21

LIST OF TABLES

Page

Table 1 Tunability of Optical Properties in Plain and Gold Particle-Coated Crumpled Graphene 22

ACKNOWLEDGEMENTS

I would like to express my most sincere gratitude to my committee chair, Professor Vasan Venugopalan, for his support and flexibility; his enthusiasm in working with students and ensuring their success is evident and enabled me to navigate through the complexities of graduate studies.

I would also like to extend my deepest appreciation to Professor Jaeho Lee, whose expertise in the field has been critical to my learning of heat transfer phenomena and whose constant guidance has been integral to my growth as an interdisciplinary researcher. His attentiveness has also ensured I make timely progress in various projects with which I am involved.

In addition, I wish to thank Professor Vojislav Stamenkovic, whose background and interest in surface modifications and nanoscale features complement well with my efforts and added new insights to the following work.

Lastly and most importantly, this work would not be possible without my family, whose wholehearted dedication to my wellbeing is paramount to my every success. To my parents and sister, thank you for always being by my side through sun and rain; this thesis is dedicated to you all.

ABSTRACT OF THE THESIS

Optical Control of Hierarchical Graphene Systems in Ultraviolet to Mid-infrared Region through Varying Surface Profiles and Nanoparticle Coatings

by

Yi Tuan

Master of Science in Chemical and Biomolecular Engineering

University of California, Irvine, 2021

Professor Vasan Venugopalan, Chair

Fundamental understanding of crumpled graphene and its optical properties are currently lacking. This paper addresses the gap in current literature by characterizing two hierarchical graphene systems: biaxially-strained randomly crumpled graphene (BRCG) and gold particle-coated periodically crumpled graphene (GP-coated PCG), through rigorous coupled-wave analysis (RCWA) and finite-difference time-domain (FDTD) computations. In BRCG, the structure is primarily characterized by its correlation length (ξ) and root-mean-square amplitude (α), which are taken as the average value over the entire simulation space, as well as the film thickness (δ). In GP-coated PCG, the periodic crumple structure is characterized by its amplitude (A) and pitch (P) as well as the radius (r) and separation (λ) of gold particles. The results show by decreasing the ξ of BRCG from 1.5 to 0.25 μm, the spectral average absorbance in the ultraviolet to near-infrared (0.2–2 μm) region increased from 0.44 to 0.75 while reflectivity was lowered from 0.52 to 0.19. Increasing α from 0.25 and 1.5 μm, the spectral average absorbance increased from 0.38 and 0.75 while reflectivity was lowered from 0.59 to 0.19. The rise in absorbance observed with decreasing ξ and increasing α is attributed to the resulting geometrically induced enhancement in internal

scattering between and within adjacent crumples. The simultaneous reduction in reflectivity is due to the amplification of interference effects and the lowering of specular reflection as surface roughness is increased. By decreasing δ from 3.5 to 0.35 nm, average absorbance was lowered from 0.45 to 0.31 due to a shorter optical length which diminishes internal scattering. Average reflectivity also increased from 0.51 to 0.66 and is driven by the reduction in absorbance. In GP-coated PCG, decreasing the P from 1 to 0.14 μm led to an increase in average solar absorbance (A_{solar}) in the UV-NIR (0.05–1 μm) region from near-zero to 0.14 due to the associated enhancement in electric field confinement and plasmonic resonance. Concurrently, the average solar transmittance (T_{solar}) in the same region decreased from 0.74 to 0.55 due to the reduced exposure of underlying transmissive graphene while the average solar reflectivity (R_{solar}) is marginally improved from near-zero to 0.05 due to the diminished separation between reflective gold particles. The same mechanisms are applied to explain the changes in optical properties with varying A. Decreasing A from 0.2 to 0.025 μm. A_{solar} increased from 0.07 to 0.14, T_{solar} decreased from 0.67 to 0.55, and R_{solar} was again marginally improved from near-zero to 0.05. In the mid-infrared (MIR, 1–20 μm), all optical signals were shifted along the wavelength axis due to Bragg diffraction without notable changes in their magnitude. Enlarging r from roughly 4.2 to 67 nm increased A_{solar} from near-zero to 0.15 due to the enhanced presence of gold particles which contribute to electric field (E-field) confinement and plasmonic resonance effects. The enlarged extinction cross-section of gold particles with increasing r also contributes to the rise in absorbance. R_{solar} also increased from near-zero to 0.09 and T_{solar} dropped from 0.74 to 0.49 due to the increased cross-section of gold particles and decreased exposure of underlying graphene, respectively. Changing λ from 0.2 to 0.05 μm, A_{solar} increased from 0.01 to 0.06 due to the enhancement in E-field confinement enabled by the closer proximity of gold particles. This was

accompanied by a reduction in T_{solar} from 0.73 to 0.67 and a marginal improvement in R_{solar} from near-zero to 0.01, attributed to the same mechanism discussed above. Marginal changes with varying particle radius and separation were observed in the MIR. Thermal analysis further demonstrates enhanced radiative heating and cooling through precisely controlling the structures' solar absorptivity and infrared emissivity. This paper presents two approaches to creating hierarchical graphene systems through varying either the surface geometry of BRCG or nanoparticle dimensions of GP-coated PCG, and subsequently tune their optical properties from the UV-NIR to MIR region to enable more effective thermal radiation control.

INTRODUCTION

Graphene and graphene-based composites have garnered much attention over the past decade. In addition to its well-known mechanical properties which establish graphene as one of the strongest and lightest materials ever discovered, it also possesses superb chemical, electrical, and thermal properties which provide it with unprecedented multifunctionality[27]. In particular, the incorporation of surface patterning, multilayer stacking, and hierarchical structuring of graphene to control its many properties is the focus of current research. Most recently, colleagues have demonstrated that the emissivity of graphene sheets in the ultraviolet (UV) and mid-infrared (MIR) region can be controlled through uniaxial mechanical crumpling. It was observed that crumpled graphene with a small (140 nm) and large pitch (10 μm) can enable emissivity control in the UV and MIR region, respectively, through variations in optical interference[14] and plasmonic resonances[11]. In similar papers, it was shown that the controlled crumpling of large-area graphene and graphene oxide (GO) gave rise to unique properties such as superhydrophobicity, tunable wettability and transmittance, and superior electrochemical activity through the introduction of hierarchical structures[5][8][21][34][39][43]. Crumpled graphene paper has further found uses as supercapacitors, owing to its excellent electrochemical properties, which were attributed to its nanoporous structure and the electrolytes contained within[36][42]. In addition, graphene-based anodes have become a viable replacement for conventional anodes in Lithium-ion batteries, combining flexibility with outstanding specific capacity, Coulombic efficiency, and cyclic stability[24][41]. Furthermore, hierarchical graphene architectures (HGAs) which rely on layer-stacking as well as self-assembly of patterned graphene were shown to have tailorable electrical transport and photovoltaic properties due to the induced changes in electron interaction[4][16][23][44]. More advanced systems which harness the diverse correlations of graphene and the effect of hierarchy have found prevalent applications across a myriad of research fields.

Hierarchically structured porous materials have been widely discussed in the energy and biomedical sectors. Such designs take advantage of graphene's high specific surface area and porosity to enable facile transport of particles, rendering them highly effective in absorption and separation, catalysis, and sensing applications as well as for energy conversion and storage[10][31][32][38]. Hierarchically wrinkled graphene has been incorporated in artificial actuators and sensors for its high conductivity and flexibility[26]. Reduced crumpled graphene oxides have been embedded within hierarchical networks of carbon nanotubes to promote efficient surface redox reactions for rapid energy storage[15] as well as significantly enhance electrical and optical properties for the development of transparent conductors[3][9][16][22][28][30][35][40][44]. Hierarchical nanostructured polymeric composites which leverage the synergistic effect between graphene oxide and select polymers have shown higher melting and crystallization temperatures as well as improved dielectric properties[20][25][37] and sensing performance[7]. Despite significant progress in the development of advanced graphene-based systems, current literature lacks a comprehensive review of the optical properties of periodically and hierarchically crumpled graphene. Existing work which discusses tunable optical properties in graphene does so within a narrow wavelength range and provides limited analysis on the effect of variation in fundamental properties[3][4][8][9][11][14][16][21][22][28][30][34][35][36][39] [40][44].

While the effect of wrinkling and crumpling of graphene has been extensively studied over the years, emphasis was mainly placed on the investigation of changes to its electronic structure and related electrochemical properties[2]. Studies which do examine the impact of crumpling on optical properties of graphene and the underlying mechanisms are scarce, while an abundance of published work can be found which discusses other materials[6]. In indium-tin-oxide thin films, biaxial crumpling led to a reduction in transmittance due to enhanced diffuse refraction[29]. In plain

PDMS films, uniaxial stretching led to a reduction in transmittance attributed to the increase in scattering loss caused by the formation of cracks at the surface[19]. In 2D inorganic compounds known as MXenes, hierarchical crumpling greatly improved light absorption due to the promotion of multiple internal reflection[17]. In general, a more crumpled surface leads to lower reflectance and higher absorbance due to the enhancement in diffuse reflection at the surface and promotion of internal reflection between adjacent peaks, respectively[33]. Destructive interference also contributes to the reduction in reflection loss, which becomes more significant with increased crumpling due to the creation of additional interfaces. The same crumpling can further improve either transmission or absorption by directing additional light into the sample. The role of surface roughness is thus implied. In discussing graphene, much attention was and continues to be given to exploring the effect of crumpling on surface plasmonic phenomenon. Increasing the crumple height in graphene resonators led to larger cavities between adjacent peaks which allow efficient trapping of photons and thus enhanced absorption at resonance wavelengths[13]. Incorporating surface particles to hierarchical ZnO nanostructures has shown to further enhance optical absorption due to localized surface plasmon resonance effect[1]. The integration of gold nanoparticles in 3D crumpled graphene has demonstrated enhanced emission for high-sensitivity spectroscopy through plasmonic field confinement[17]. Plasmonic resonance and the associated absorption peaks can also be tuned through nanoscale crumpling of graphene[11]. While the above mechanisms pertaining to graphene are well-studied, the rudimentary relationship between geometric parameters and optical properties has not been thoroughly presented. This paper will provide a fundamental analysis on the effect of characteristic parameters, including pitch, amplitude, thickness, and particle size as well as distribution on the optical properties of either hierarchically crumpled graphene or gold particle-coated biaxially-crumpled graphene. Key

mechanisms which drive changes in optical properties will be identified and discussed to provide a comprehensive understanding of basic graphene-based designs which is currently lacking.

In this work, a thorough analysis of two structures: biaxially-strained randomly crumpled graphene and gold particle-coated periodically crumpled graphene, will be presented. The effect of characteristic parameters, including pitch, amplitude, number of layers, and particle size and distribution, on reflectivity, transmittance, and absorbance will be discussed. The results from the UV to NIR region (0.2–2 μm) will be presented for biaxially-strained randomly crumpled graphene and from the UV to MIR region (0.05–20 μm) for gold particle-coated periodically crumpled graphene. Furthermore, to identify potential thermal management applications, temperature predictions will be performed and discussed in the context of changes in optical properties.

CHAPTER 1

BIAXIALLY-STRAINED RANDOMLY CRUMPLED GRAPHENE

1.1 Sample Geometry and Computational Methods

The first structure investigated is the biaxially-strained randomly crumpled graphene (Fig. 1a). To simulate this structure, the "rough surface" object in FDTD was used (Fig. 1b), which is primarily characterized by two parameters: root-mean-square amplitude (α) and correlation length (ξ), which roughly corresponds to amplitude and pitch, respectively, in periodic systems. As such, α and ξ are taken as the average of the amplitude and pitch of all individual crumples within the simulated region. The investigated structure consists of five-layer graphene with a thickness of 1.75 nm on top of a semi-infinite copper substrate with a thickness of 1 μm. A 2 x 2 μm unit cell was simulated with a vertically injected plane wave source along the vertical axis. Periodic boundary conditions were imposed in both x- and y-direction, while a perfectly matched layer (PML) was applied in the vertical z-axis. As an initial estimate, α and ξ were both set to 0.25 μm. In the following section, the effect of varying α and ξ from 0.25 to 1.50 μm will be determined. Afterwards, thickness will also be varied between 0.35 and 3.5 nm, corresponding to mono- and ten-layer graphene, respectively.

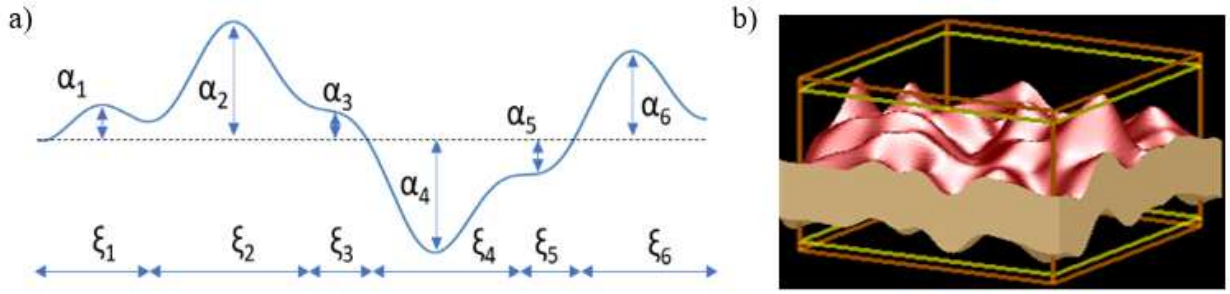

Figure 1: (a, left) Schematic and (b, right) simulation object in FDTD of biaxially-strained randomly crumpled graphene. The simulated system consists of 5-layer graphene with a thickness of 1.75 nm on a 1 μm thick semi-infinite copper substrate. A 2x2 μm unit cell was simulated with a vertically injected plane wave source. Periodic boundary conditions were imposed in horizontal plane, while a perfectly matched layer (PML) was applied in the vertical direction. The correlation length (ξ) and RMS amplitude (α) are both set to 0.25 μm for the default case.

1.2 Optical Properties

1.2.1 Variation in Correlation Length (ξ) and Root-Mean-Square Amplitude (α)

The spectral average absorbance of biaxially-strained randomly crumpled graphene as a function of aspect ratio (AR = α/ξ) for three different fixed correlation lengths (ξ = 0.25, 0.75, 1.50 μm) is plotted in Figure 2. The RMS amplitude (α) was varied between 0.25, 0.75 and 1.50 μm to incur the changes in AR. Figure 2a indicates a clear logarithmic-like growth in absorbance with increasing aspect ratio. Minimizing ξ from 1.50 to 0.25 μm and maximizing α from 0.25 to 1.5 μm led to the most significant rise in spectral average absorbance from 0.18 to its highest value of 0.75. The increase in absorbance with larger aspect ratios can be attributed to the resulting enhancement in internal scattering between adjacent peaks. The contour plot in Figure 2b illustrates the impact of α and ξ on absorbance. The bright yellow spot in the upper left corner corresponds to the highest average absorbance and is associated with optimal heating, while the dark blue region near the bottom right corner indicates the minimization of absorbance to achieve optimal cooling.

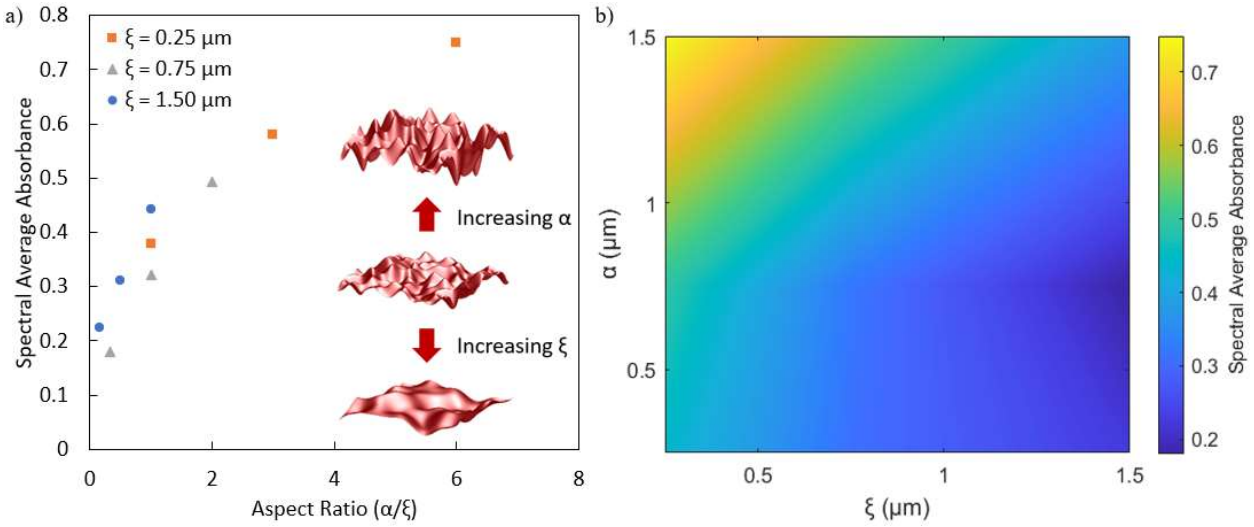

Figure 2: (a) Spectral average absorbance of biaxially-strained randomly crumpled graphene as a function of aspect ratio for three different fixed correlation lengths (ξ = 0.25, 0.75, 1.50 μm) obtained through FDTD simulations. The various points of the same color correspond to changing RMS amplitudes (α = 0.25, 0.75, 1.50 μm). A clear logarithmic-like growth in absorbance with increasing aspect ratio is observed. Minimizing ξ from 1.50 to 0.25 μm

and maximizing α from 0.25 to 1.5 μm led to the most significant rise in spectral average absorbance from 0.18 to its highest value of 0.75. (b) Contour plot showing the dependence of absorbance on α and ξ. The 9 solutions shown in part (a) are obtained through FDTD simulations and used along with interpolation by MATLAB to generate the intermediate datapoints. The bright yellow region in the top left corner indicates the maximization of solar absorbance to above 0.7 for optimal heating. In contrast, the dark blue region near the bottom right corner suggests the minimization of solar absorbance to near 0.2 if optimal cooling is desired.

The effect of varying α and ξ on reflectivity, transmittance, and absorbance are shown in more details in Supplementary. Average reflectivity was reduced from 0.78 to 0.19 with increasing α and decreasing ξ. The reduction in reflectivity with increasing α and decreasing ξ is attributed to the enhancement in surface roughness and thus diffuse reflection. A marginal decrease in transmittance was observed with lower α for all ξ cases, mainly between 0.2 and 0.25 μm. This may be due to the increase in incident angle which directs additional photons into the sample. With decreasing α and increasing ξ, one observes a minor decrease in transmittance between 0.2 and 0.25 μm. Beyond 0.25 μm, transmittance drops to zero when ξ exceeds 0.75 μm (Fig. S1).

1.2.2 Variation in Thickness (δ)

For the previous analysis, the thickness (δ) of the samples was kept at 1.75 nm, corresponding to five layers of graphene. Here δ was varied between 0.35, 1.05, 1.75, and 3.5 nm, equivalent to mono-, three-, five- and ten-layer graphene, respectively. A general increase in absorbance across the entire spectrum, most significantly between 0.5 and 2 μm, was observed in Figure 3a. The enhanced absorbance as well as reduced reflectivity are attributed to the increase in scattering events which occur with larger thicknesses. It can also be seen that the absorbance peaks in the visible range between 0.2 and 0.5 μm remain significant regardless of how many layers are present. Due to the opaque and semi-infinite copper substrate, transmittance is negligible and thus the increase in absorbance is exactly mirrored by a decrease in reflectivity. Figure 3b plots the spectral average absorbance and reflectivity as a function of thickness. A nearly linear increase (decrease) in absorbance (reflectivity) can be clearly observed. It can be summarized that

by enlarging δ from 0.35 to 35 nm, the average absorbance increased from 0.31 to 0.45 while reflectivity decreased from 0.66 to 0.51.

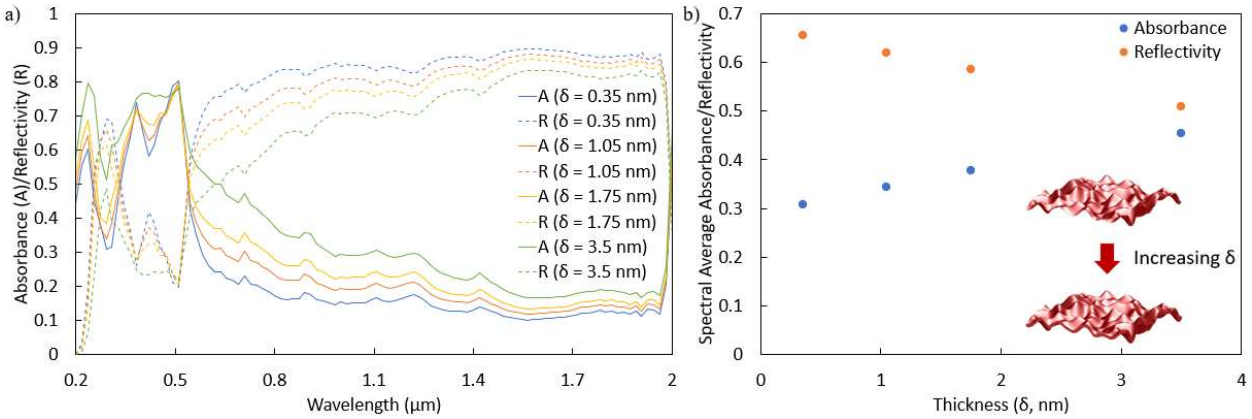

Figure 3: (a) Reflectivity and absorbance of biaxially-strained randomly crumpled graphene in the near-infrared region with varying thickness (δ = 0.35, 1.05, 1.75, 3.5 nm) obtained through FDTD simulations. (b) Spectral average values of the reflectivity and absorbance solutions shown in (a) as a function of thickness. Both the correlation length and RMS amplitude was set to their default value of 0.25 μm. By enlarging δ from 0.35 to 35 nm, the average absorbance increased from 0.31 to 0.45 while reflectivity decreased from 0.66 to 0.51. An increase in absorbance was observed in thicker samples due to the increase in optical path length and thus photon scattering, which also reduces reflectivity. Transmittance data was not shown since it is negligible due to the opaque and semi-infinite copper substrate. A nearly linear increase (decrease) in absorbance (reflectivity) can be clearly observed in (b).

CHAPTER 2

GOLD PARTICLE-COATED PERIODICALLY CRUMPLED GRAPHENE

2.1 Sample Geometry and Computational Methods

The second structure is gold particle-coated periodically crumpled graphene and was generated in FDTD with four primary parameters: pitch (P), amplitude (A), particle radius (r), and particle separation distance (λ). The last parameter refers to the distance in the x- and y-direction of the horizontal plane between adjacent gold particles. The unit cell consists of five gold particles each with radius r evenly distributed along the x direction of crumpled 10-layer graphene with a thickness of 3.5 nm and specified aspect ratio A/P. For the analysis of λ, the number of gold particles was changed accordingly between three and nine. The simulation conditions remain mostly identical between simulations except for the unit cell dimension. The x span of the unit cell was set equal to P while the y span was set to P/4 in order to ensure proper crumpling periodicity. The radius (r) of the gold particles was initially set to 16.75 nm (R). The schematic as well as the simulation object in FDTD for this structure are shown in Figure 4. The values for P, A, r, and λ were varied and the effect on optical and thermal properties determined. P was varied from 0.14 to 1 μm, which essentially simulates a flat geometry; A was changed from 0.025 to 0.2 μm; r was changed from a R/4 to 4R, or from 4.1875 to 67 nm; and λ was varied from 0.1 to 0.4 μm. The results in the ultraviolet to near-infrared region (UV-NIR, 0.05–1 μm) will be presented first followed by those in the mid-infrared region (MIR, 1–20 μm).

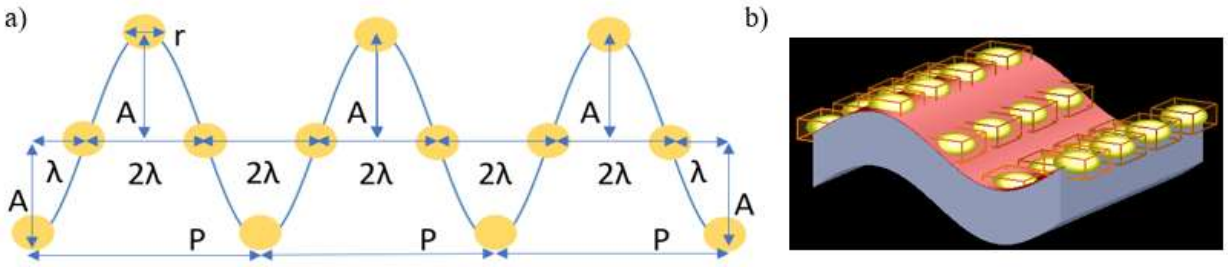

Figure 4: (a, left) Schematic and (b, right) simulation object in FDTD of gold particle-coated periodically crumpled graphene. The default pitch (P) was 0.2 μm, amplitude (A) was 0.2 μm, particle radius (r) was 16.75 nm, and particle separation (λ) was 0.1 μm. The unit cell consists of five gold particles each with radius r evenly distributed along the x direction of crumpled 10-layer graphene with a thickness of 3.5 nm and specified aspect ratio A/P. Periodic boundary conditions were applied in both the x- and y-direction while a perfecting matching layer was applied in the vertical (z) direction. A vertically injected plane wave source was used. The x and y span of the unit cell was set to P and P/4 to cover one full period of the simulation object and ensure proper crumpling periodicity.

2.2 Sample Geometry and Computational Methods

2.2.1 Variation in Amplitude (A) and Pitch (P)

The spectral average UV-NIR (0.05–1 μm) absorbance of gold particle-coated periodically crumpled graphene as a function of aspect ratio (AR = A/P) for six different fixed pitch dimensions (P = 0.14, 0.2, 0.4, 0.6, 0.8, 1 μm) is plotted in Figure 5. The amplitude (A) was varied between 0.025, 0.05, 0.1, and 0.2 μm to incur a change in AR for a given P. The effect of changing A and P on the sample structure is shown in Figure 5a. The individual curves in Figure 5b reveal a clear increase in absorbance with decreasing amplitude, or a smaller AR, which is attributed to the closer proximity of gold particles and the resulting enhancement in electric field confinement. The same mechanism can explain the increase in absorbance with decreasing pitch, which can be readily observed by comparing the different curves of Figure 5b. By decreasing A from 0.2 to 0.025 μm and P from 1 to 0.14 μm, average absorbance was increased from near-zero to a maximum of 0.14 in the UV-NIR region due to the closer proximity of gold particles and the resulting enhancement in electric field confinement. Simultaneously, average transmittance is reduced from 0.74 to 0.55 due to the diminished exposure of underlying transmissive graphene (Fig. S8a). Average reflectivity is marginally improved by 0.05 as the gold particles move closer to each other (Fig.

S8b). It can be noted that the change in absorbance is more significant with smaller pitch values due to the larger change in aspect ratio when the amplitude is varied (Fig. S4). For a pitch of 0.14 μm, the spectral average absorbance increased by 0.074, compared to only 0.0013 for a pitch of 1 μm, when A decreased from 0.2 to 0.025 μm (Fig. 5b). Similar behavior is observed in reflectivity and transmittance (Fig. S2,S3). Looking instead at the effect of varying pitch with a fixed amplitude, its effect on absorbance becomes less significant at larger amplitudes, as demonstrated by the logarithmic-like curves of Figure 5b and S4. For an amplitude of 0.025 μm, the spectral average absorbance increased by 0.136, compared to only 0.064 for an amplitude of 0.2 μm, when P was decreased from 1 to 0.14 μm (Fig. S7). The same occurs for reflectivity and transmittance (Fig. S5,S6). This indicates the limitation of controlling reflectivity, transmittance, and absorbance through amplitude alone. The above observations regarding the changing significance of variation in pitch and amplitude suggest that to effectively tune the optical properties of gold particle-coated periodically crumpled graphene, both P and A need to be considered. The contour plot shown in Figure 5c provides a better visualization of the effect of A and P on absorbance. A bright yellow spot appears in the lower left corner which corresponds to the highest average absorbance of 0.14 and demonstrates the optimal design for radiative heating, while the dark blue region on the far right indicates the minimization of absorbance for optimal cooling.

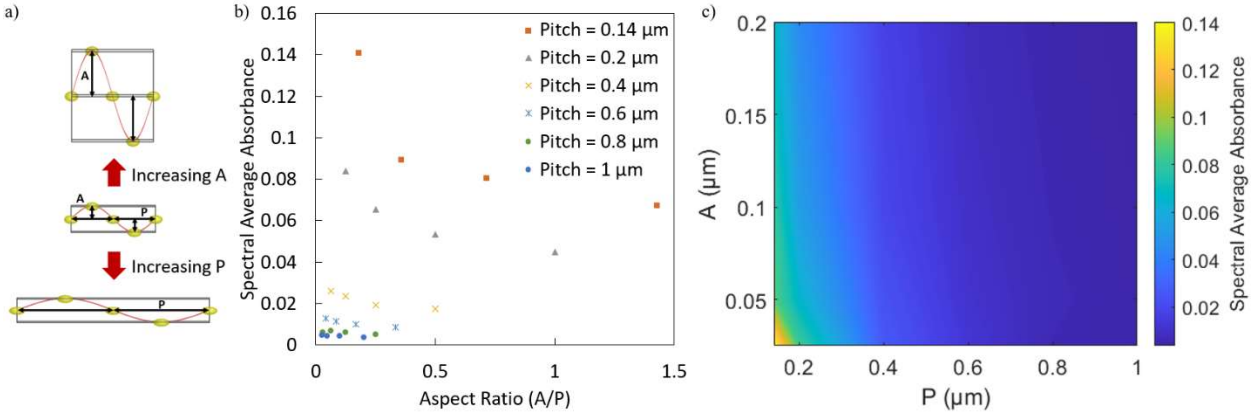

Figure 5: (a-c) Effect of changing amplitude (A) and pitch (P) on the structure and absorbance in the ultraviolet-near-infrared (UV-NIR, 0.05–1 µm) region of gold particle-coated periodically crumpled graphene. (b) Spectral average absorbance of the sample in UV-NIR region as a function of aspect ratio for six different fixed pitch values (P = 0.14, 0.2, 0.4, 0.6, 0.8, 1 µm). The various points of the same color correspond to changing amplitudes (A = 0.025, 0.05, 0.1, 0.2 µm). With decreasing A and P, average absorbance was increased from near-zero to a maximum of 0.14 due to the closer proximity of gold particles and the resulting enhancement in electric field confinement. Simultaneously, average transmittance is reduced by 0.19 (Fig. S3) and average reflectivity is marginally improved by 0.05 (Fig. S2). (c) Contour plot showing the dependence of absorbance on amplitude and pitch. The 24 solutions shown in (a) are obtained through FDTD simulations and used along with interpolation by MATLAB to generate the intermediate datapoints. A bright yellow spot appears in the lower left corner which corresponds to the highest average absorbance of 0.14 and demonstrates the optimal design for radiative heating, while the dark blue region on the far right indicates the minimization of absorbance for optimal cooling.

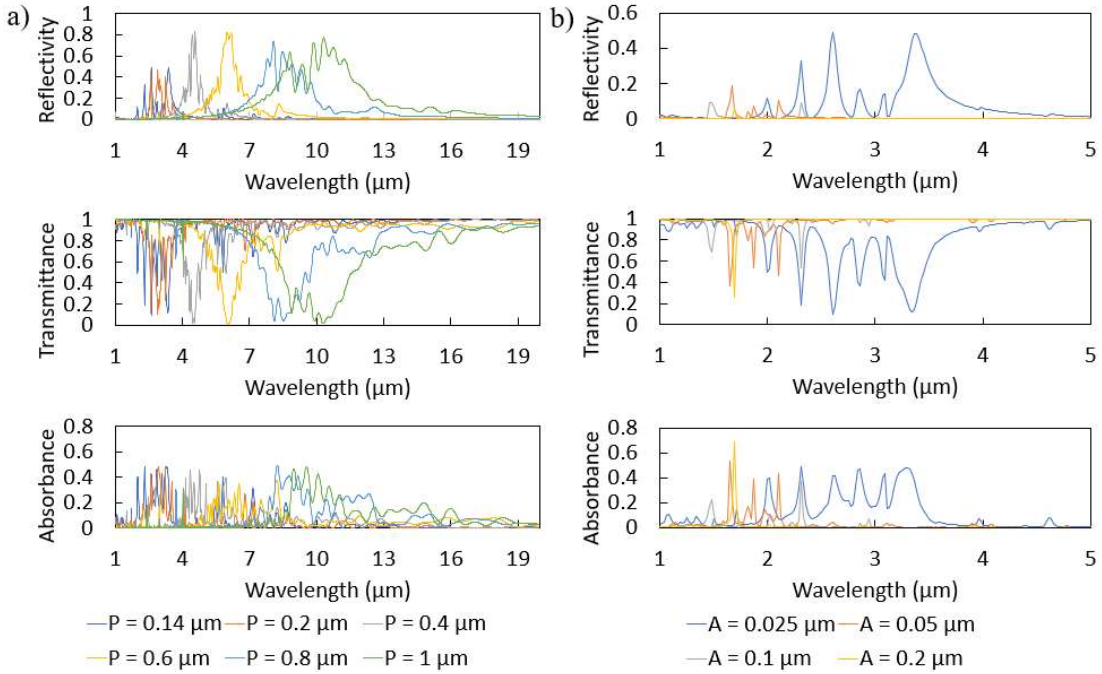

Figure 6: (a-b) Reflectivity, transmittance, and absorbance of gold particle-coated periodically crumpled graphene in the mid-infrared (MIR) region with varying pitch (P = 0.14, 0.2, 0.4, 0.6, 0.8, 1 µm) and amplitude (A = 0.025, 0.05, 0.1, 0.2 µm) obtained through FDTD simulations. (a) Increasing P led to a notable shift in all optical signals towards higher wavelengths due to the increase in apparent distance between gold particles, which is consistent with Bragg's Law. (b) Similarly, increasing A led to a shift in optical peaks towards lower wavelengths due to the decrease in apparent distance between gold particles. Varying either P or A led to mostly negligible changes in the magnitude of

optical signals, although decreasing A to 0.025 μm led to a considerable increase in reflectivity to nearly 0.5 between 2 and 4 μm. These results are significant as they demonstrate tunability of optical properties in the MIR region.

In the MIR region, all signals: reflectivity, transmittance, and absorbance (Fig. 6), are redshifted with larger P values. This is consistent with Bragg's Law, which states that the wavelength of scattered light is proportional to the apparent distance between particles. Thus, by increasing P, the apparent distance between gold particles becomes larger, resulting in a shift in optical signals towards longer wavelengths. Similarly, all signals below 5 μm are blueshifted with increasing A. As the amplitude increases, the apparent distance between the surface gold particles decreases and so does the resultant wavelength. No discernable trends were observed above 7 μm. Varying either P or A led to mostly negligible changes in the magnitude of optical signals, although decreasing A to 0.025 μm led to a considerable increase in reflectivity to nearly 0.5 between 2 and 4 μm (Fig. 6b). The shift in signals is significant since it demonstrates tunability of optical properties in the MIR region which could be leveraged to design more efficient selective emitters and other wavelength-specific devices.

2.2.2 Variation in Particle Radius (r)

The effect of particle radius in the UV to NIR region is presented in Figure 7. Two different pitch values were considered: 0.4 and 1 μm. For both cases, as r is lowered and the gold particles decrease in size, the sample begins to resemble plain crumpled graphene and becomes mostly transmissive as both reflectance and absorbance reduce to zero within the UV-NIR region. For a pitch of 0.4 μm, as r was lowered from 33.5 (2R) to 8.375 nm (R/2), average transmittance increased from 0.55 to 0.74 while average reflectivity and absorbance decreased from 0.06 and 0.14, respectively, to effectively zero. For a pitch of 1 μm, as r was lowered from 67 (4R) to 4.1875 nm (R/4), average transmittance increased from 0.49 to 0.74 while average reflectivity and absorbance decreased from 0.09 and 0.15, respectively, to zero (Fig. 7, S9). With decreasing r,

reflectivity is lowered due to the decreased presence of reflective gold particles, while absorbance is suppressed due to diminishing electric field confinement along the crumpled graphene surface. Comparing between the low and high pitch cases, it can be seen that a proportionally greater change in particle radius is required to incur a similar change in optical properties than for a lower pitch. This was expected since the optical properties of particle-coated structures are largely dependent on the relative presence between the particles and the underlying substrate.

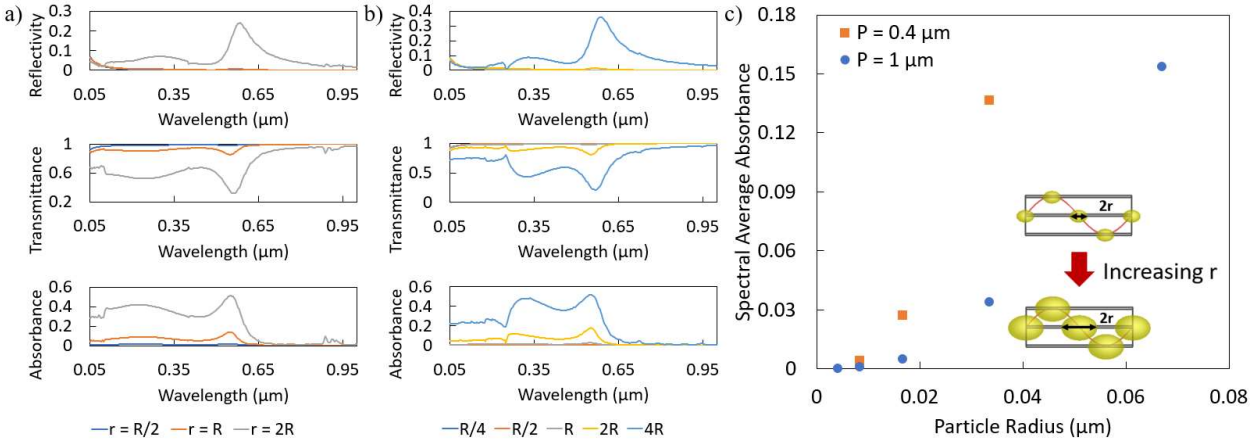

Figure 7: (a,b) Reflectivity, transmittance, and absorbance of gold particle-coated periodically crumpled graphene in the ultraviolet-near-infrared (UV-NIR) region with varying gold particle radius (r = 4.1875 (R/4), 8.375 (R/2), 16.75 (R), 33.5 (2R), 67 nm (4R)) for two different pitch values (P = 0.4, 1 μm) obtained through FDTD simulations. (c) Spectral average absorbance in the NIR as a function of particle radius for the two different pitch values. (a) For a pitch of 0.4 μm, a smaller radius range (r = 8.375 (R/2), 16.75 (R), 33.5 nm (2R)) was applied due to geometrical constraints. (b) For a larger pitch of 1 μm, the full range was explored. (c) For a pitch of 0.4 μm, with smaller r, average transmittance increased from 0.55 to 0.74 while average reflectivity and absorbance decreased from 0.06 and 0.14, respectively, to effectively zero. For a pitch of 1 μm, with smaller r, average transmittance increased from 0.49 to 0.74 while average reflectivity and absorbance decreased from 0.09 and 0.15, respectively, to zero (Fig. S9). As r decreases, the sample approaches plain crumpled graphene and becomes increasingly transmissive while reflectivity is lowered due to the decreased presence of reflective gold particles and absorbance is suppressed due to diminishing electric field confinement. Note that for a larger pitch, a proportionally greater change in particle radius is required to incur the same change in optical properties than for a lower pitch.

In the MIR region, no significant changes in the magnitude of optical signals were observed (Fig. 8). Comparing the low and high pitch case, one sees generally similar features, however, those for the large pitch case occur at much higher wavelengths than for the low pitch case. For P = 0.4 μm, the optical signals appear between 3 and 7 μm. For P = 1 μm, the same features occur between 4 and 19 μm. This shift in signals may be explained in terms of Bragg's shift and again

demonstrates tunability of MIR reflectivity, transmittance, and absorbance for thermal management applications.

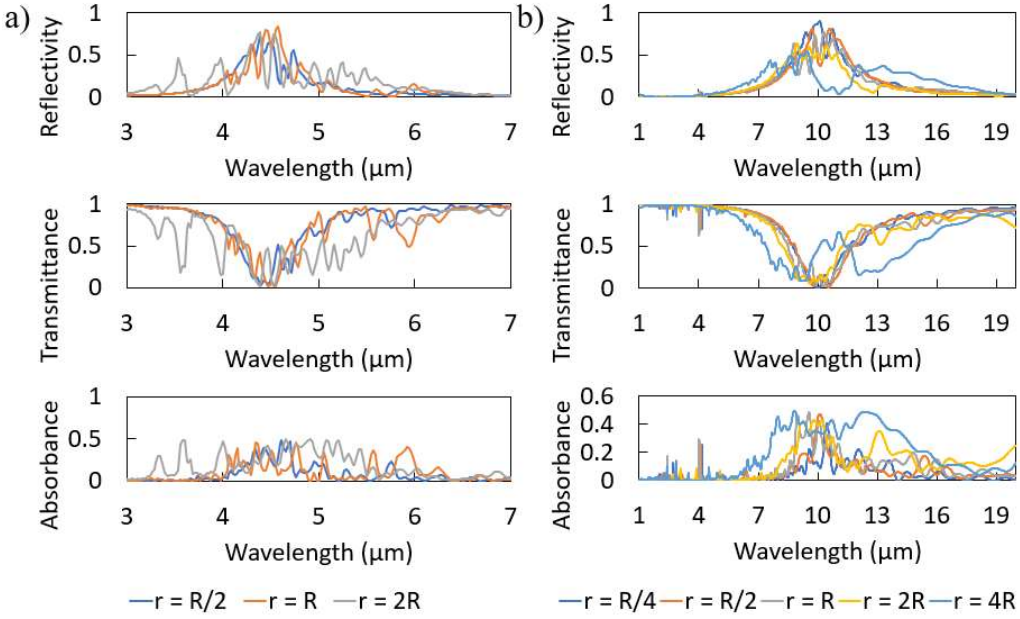

Figure 8: (a,b) Reflectivity, transmittance, and absorbance of gold particle-coated periodically crumpled graphene in the mid-infrared (MIR) region with varying particle radius (r = 4.1875 (R/4), 8.375 (R/2), 16.75 (R), 33.5 (2R), 67 nm (4R)) for two pitch values (P = 0.4, 1 μm) obtained through FDTD simulations. (a) For a pitch of 0.4 μm, a smaller radius range (r = 8.375 (R/2), 16.75 (R), 33.5 nm (2R)) was applied due to geometrical constraints. (b) For a larger pitch of 1 μm, the full range was explored. No significant change trends were observed in this region. However, for the large pitch case, the features occur at larger wavelengths compared to the lower pitch case. This may be attributed to the increase in apparent distance between gold particles.

2.2.3 Variation in Particle Separation (λ)

The last parameter to be analyzed is the particle separation (λ), which corresponds to the horizontal distance between the centers of adjacent gold particles. As λ increases from 0.05 to 0.2 μm, the number of gold particles is reduced from 9 to 3, leading to an enhancement in average transmittance of around 0.06 as well as a reduction in absorbance by 0.05 in the UV to NIR region (Fig. 9a,c). The higher transmittance arises from the increased area of exposed graphene, while the lower absorbance is attributed to the reduction in electric field confinement between gold particles, which are further apart from each other with increasing λ. A marginal decrease in reflectivity of around 0.01 was also observed due to the decrease in number of reflective gold particles (SI). In

the MIR region, only minor effects were observed (Fig. 9b). However, major absorbance peaks as high as 0.45 appear between 10 and 17 μm when λ is minimized to 0.05 μm due to stronger electrical field confinement and enhanced internal scattering.

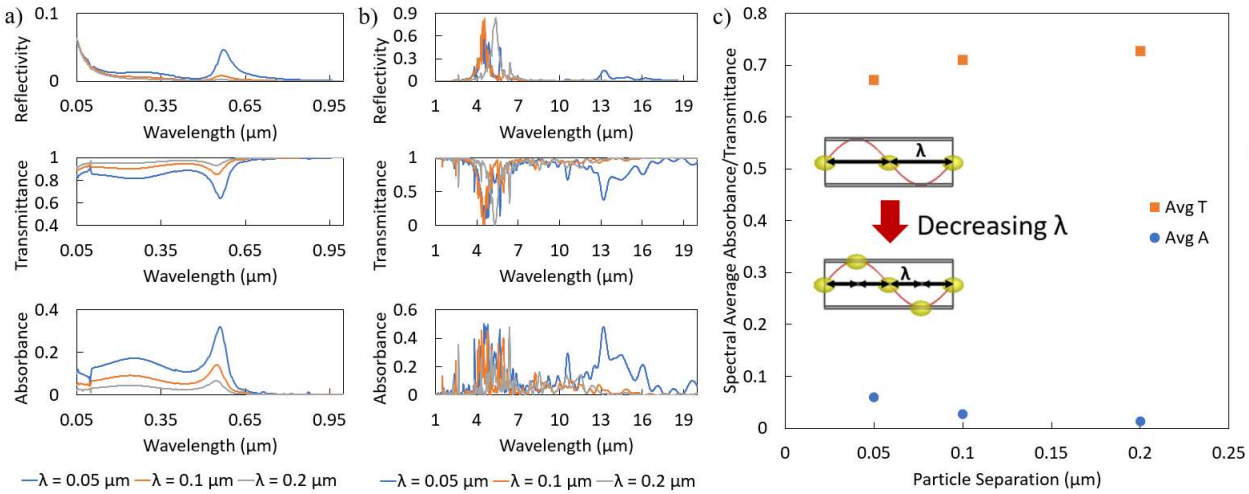

Figure 9: (a,b) Reflectivity, transmittance, and absorbance of gold particle-coated periodically crumpled graphene in the ultraviolet-near-infrared to mid-infrared (UV-NIR to MIR) region with varying gold particle separation (λ = 0.05, 0.1, 0.2 μm) obtained through FDTD simulations. (c) Spectral average absorbance and transmittance in the UV-NIR as a function of particle separation. (a,c) As λ increases from 0.05 to 0.2 μm, the number of gold particles is reduced from 9 to 3, leading to an enhancement in average transmittance by 0.06 due to the increased area of expose graphene, which is transmissive. A reduction in average absorbance from 0.06 to 0.01 was also observed when the gold particles are further apart from each other, corresponding to a larger λ, due to the reduction in electric field confinement. This trend is better visualized in (c). A marginal decrease in reflectivity of 0.01 was observed due to the reduced number of reflective gold particles (SI). (b) In the MIR region, no clear trends are present, although major absorbance peaks appear between 10 and 17 μm when λ is minimized due to stronger electrical field confinement and enhanced internal scattering.

2.3 Optimization of Design

To conclude the analysis of the discussed geometric parameters (Pitch, amplitude, particle radius, particle separation) for gold particle-coated periodically crumpled graphene, their values are optimized and presented in terms of electric field confinement (Fig. 10). Radiative heating was demonstrated here, although the same optimization process can be applied for radiative cooling. Figure 10 plots the cross-sectional electric field (V/m) in the x-z plane for various designs and indicates an optimal geometric configuration for maximal solar absorbance in gold particle-coated periodically crumpled graphene. All geometric dimensions for designs A through D are set equal to those of the optimized design E except for the parameter indicated. With a larger pitch (P) of

0.4 μm, the gold particles are not sufficiently near each other to support proper confinement of electric field (Fig. 10a). The same behavior can be observed for a larger amplitude (A) of 0.2 μm (Fig. 10b) and particle separation (λ) of 0.07 μm (Fig. 10c). Reducing the radius (r) of the gold particles by a factor of four allows for confinement, however, the magnitude and area of the confined field is notably reduced (Fig. 10d). The optimal design clearly shows the highest level of electric field confinement between the gold particles, with a magnitude of at least 3 V/m on average and exceeding 6 V/m at multiple locations (Fig. 10e). Figure 10f provides a comparison of the solar absorbance for all five designs presented. Design E offers the highest absorbance across nearly the entire spectrum, reaching 0.46 at a wavelength of 0.565 μm, and can be directly attributed to the maximization of electric field confinement.

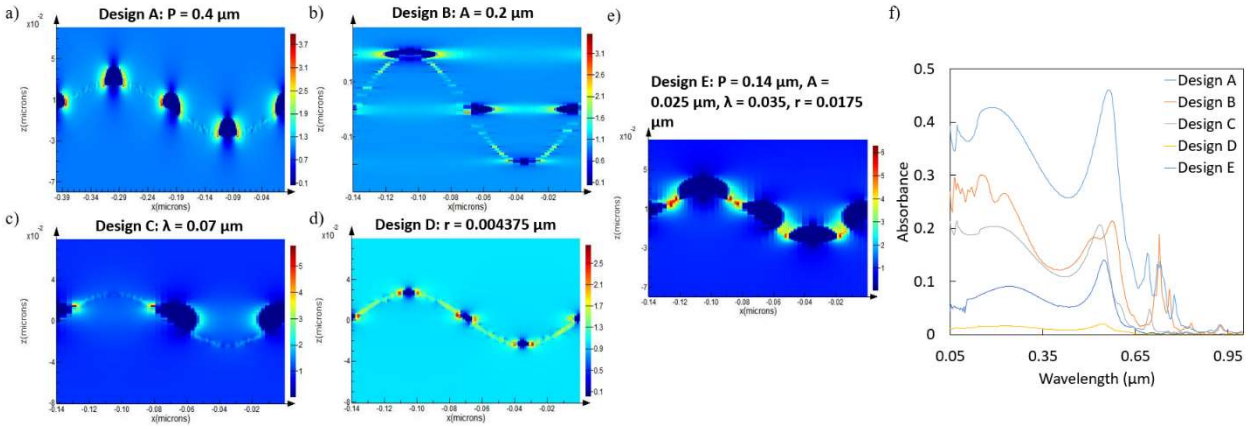

Figure 10: (a-e) Plots of the cross-sectional electric field (V/m) in the x-z plane and (f) corresponding solar absorbance indicate an optimal geometric configuration for maximal heating in gold particle-coated periodically crumpled graphene. All geometric dimensions are set equal to those of the optimal design except for the parameter indicated. (a) With a larger pitch (P) of 0.4 μm, the gold particles are not sufficiently near each other to support proper confinement of electric field. The same behavior can be observed for (b) a larger amplitude (A) of 0.2 μm and (c) particle separation (λ) of 0.07 μm. (d) Reducing the radius (r) of the gold particles by a factor of four allows for confinement, however, the magnitude and area of the confined field is reduced. (e) The optimal design clearly shows the highest level of electric field confinement between the gold particles, with a magnitude of at least 3 V/m on average and exceeding 6 V/m at multiple locations. (f) Comparison of the solar absorbance for the various designs. Design E offers the highest absorbance across nearly the entire spectrum, reaching a maximum of 0.46 at a wavelength of 0.565 μm.

CHAPTER 3

THERMAL PROPERTIES

To determine potential radiative cooling applications for both biaxially-strained randomly crumpled graphene and gold particle-coated periodically crumpled graphene, the temperature profile of all samples presented were computed using a custom code in MATLAB. The code obtains the temperature over a 24-hour period by solving an energy balance consisting of four terms: incoming solar radiation, incoming atmospheric radiation, outgoing sample radiation, and convective heat loss. Typical terrestrial ambient temperature, atmospheric transmittance, and solar irradiance data were applied as boundary conditions along with the effective heat transfer coefficient (h), which was assumed to be 10 W/m^2K for all temperature calculations performed.

3.1 Biaxially-strained Randomly Crumpled Graphene

The effect of varying the RMS amplitude (α) and correlation length (ξ) on the radiative cooling performance of randomly crumpled graphene is shown in Figure 11a. It can be observed by comparing curves of different colors that for most ξ values, as α decreased from 1.50 to 0.25 μm, the sample's daytime temperature became significantly lower. The same reduction in temperature can be generally observed by comparing solid and dashed curves, specifically as ξ increases from 0.25 to 1.50 μm. Minor deviations were seen for cases where α is large. The maximum temperature reduction attained was roughly 15 ^oC by reducing α from 1.50 to 0.25 μm and maintaining ξ at 0.75. The reduction in temperature with lower α and higher ξ can be directly attributed to the corresponding decrease in absorbance in the solar region (0.2–2 μm) as shown by Figure 2.

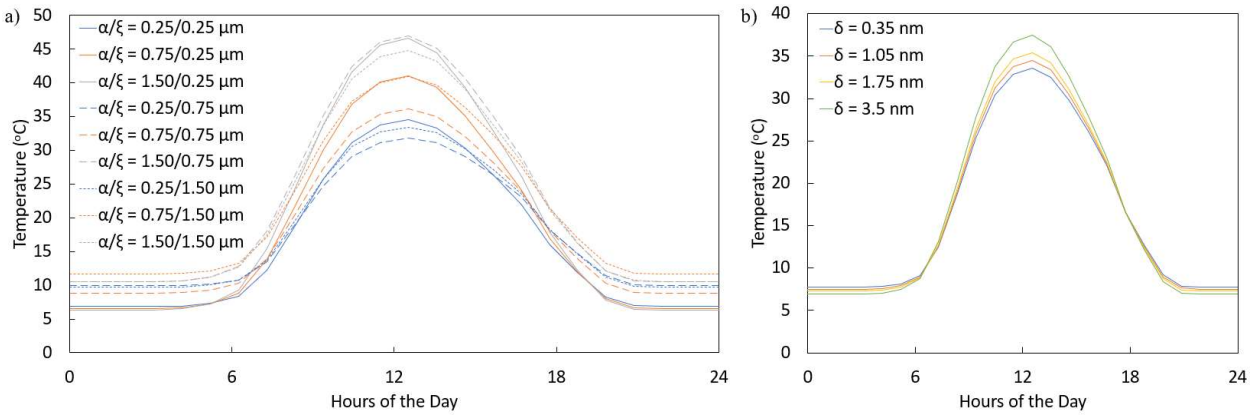

Figure 11: (a) Effect of correlation length (ξ), RMS amplitude (α), and (b) thickness on radiative cooling performance of biaxially-crumpled randomly crumpled graphene obtained through MATLAB. Typical terrestrial ambient temperature, atmospheric transmittance, and solar irradiance values were applied. An effective heat transfer coefficient (h) of 10 W/m^{2}K was used. The same boundary conditions were used for all temperature analysis presented in this paper. In general, a reduction in sample temperature was observed for lower α and larger ξ and is attributed to the accompanied decrease in solar absorbance. The maximum temperature reduction attained was roughly 15 °C by reducing α from 1.50 to 0.25 μm and maintaining ξ at 0.75. With a smaller number of layers, corresponding to a thinner sample, the temperature was reduced by roughly 4 °C due to the accompanied decrease in solar absorbance.

Regarding the effect of thickness on radiative cooling, one sees in Figure 11b a reduction in temperature by 4 °C upon decreasing the thickness from 3.5 to 0.35 nm due to the resulting increase in absorbance within the solar region (Fig. 3). For the thinnest possible sample, corresponding to monolayer graphene, the sample temperature was still above that of ambient, suggesting that plain randomly crumpled graphene with the specified dimensions could not achieve subambient cooling.

3.2 Gold Particle-coated Periodically Crumpled Graphene

The effect of pitch on radiative cooling is shown in Figure 12a. As the pitch increases, the sample can remain at lower temperatures due to the corresponding decrease in solar absorbance (Fig. 5b, c) and redshift in MIR absorbance beyond the solar region (Fig. 6a), leading to less energy absorbed from incoming solar radiation. With an amplitude of 0.025 μm, increasing the pitch from 0.14 to 1 μm reduced the daytime temperature by 7.1 °C. The observed temperature reduction gradually diminishes at larger amplitudes (Fig. S10). For an amplitude of 0.2 μm, the same increase

in pitch reduced the daytime temperature by only 3.6 °C. Furthermore, when the pitch exceeds 0.8 μm, near-ambient cooling was achieved during the day under the specified simulation conditions.

The effect of amplitude on radiative cooling is shown in Figure 12b. With a pitch of 0.14 μm, increasing the amplitude from 0.025 to 0.2 μm led to a slight rise in solar transmittance which drives a corresponding decrease in solar absorbance (Fig. 5b, c) and daytime temperature of 3.9 °C. The predicted temperature reduction gradually diminishes at larger amplitudes and becomes marginal when the pitch exceeds 0.4 μm (Fig. S11). In conjunction with the same observation with regards to pitch, it can be noted that more effective optical and thermal control is attained at lower geometric dimensions.

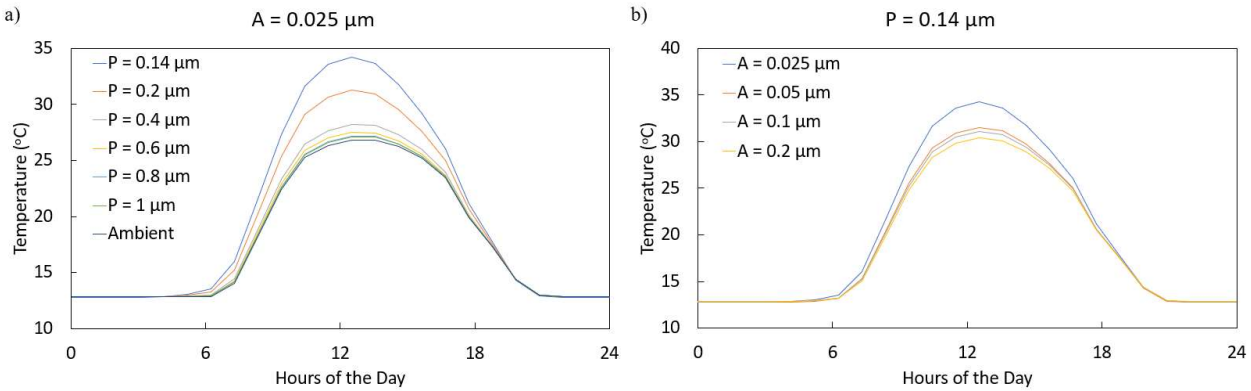

Figure 12: (a) Effect of pitch (P) and (b) amplitude (A) on radiative cooling performance of gold particle-coated periodically crumpled graphene obtained through MATLAB. (a) With A being 0.025 μm, increasing P from 0.14 to 1 μm reduced the daytime temperature by over 7 °C due to the accompanied decrease in solar absorbance. When P exceeds 0.8 μm, near-ambient cooling was achieved during the day under the specified simulation conditions. (b) With P being 0.14 μm, by increasing A from 0.025 to 0.2 μm, corresponding to a low solar absorbance, temperature was reduced by nearly 4 °C. The change in temperature became marginal when the amplitude was reduced to below 0.05 μm. The A and P value shown in (a) and (b), respectively, were chosen since they demonstrated maximum temperature reduction, whose effect is gradually diminished with larger A and P value in their corresponding analysis.

In discussing the effect of particle radius on radiative cooling, two cases were considered: a highly crumpled sample with a pitch of 0.14 μm and a nearly flat sample with a pitch of 1 μm. For a small pitch value of 0.14 μm, the temperature decreased by 6.9 °C during daytime and remained mostly invariant during nighttime when the particle radius was decreased from 33.5 to 8.375 nm (Fig. 13a). For a large pitch value of 1 μm, the same effect is observed, although a larger

change in particle radius, from 67 to 4.1875 nm, was required to reach a similar reduction in temperature of 8.1 ºC (Fig. 13b). The decrease in temperature is attributed to the decreased absorbance in the solar region with smaller particle radius.

The effect on particle separation on radiative cooling is shown in Figure 12c. As expected, due to their reduced solar absorption, samples with higher particle separation distance reached lower daytime temperatures. Increasing the particle separation from 0.05 to 0.2 μm reduced the temperature by 2.5 ºC.

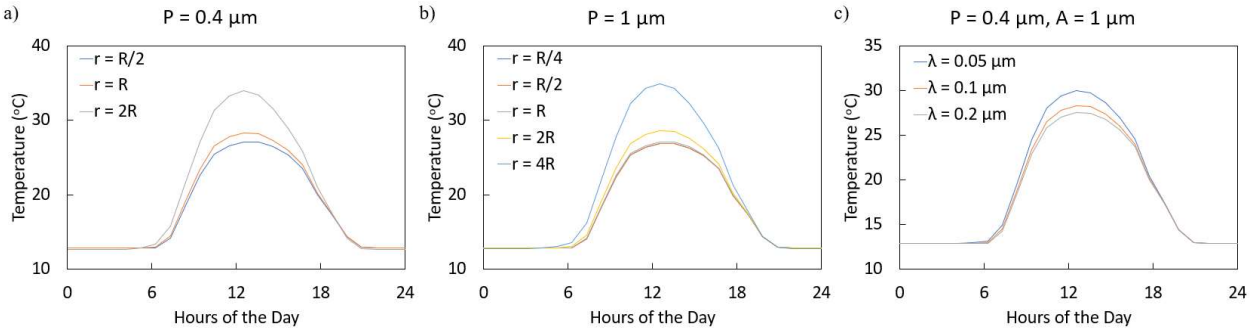

Figure 13: (a, b) Effect of particle radius (r) and (c) particle separation (λ) on radiative cooling performance of gold particle-coated crumpled graphene obtained through MATLAB. Amplitude was set to 0.025 μm for the analysis of r and 1 μm for the analysis of λ. (a) For a pitch of 0.14 μm, r was varied between 8.375 nm (R/2) and 33.5 nm (2R), which is near the maximum size allowed for the given pitch without overlapping of particles. (b) For a pitch of 1 μm, r was varied between 4.1875 nm (R/2) and 67 nm (2R). Decreasing r from 2R to R/2, the temperature was reduced by around 7 ºC due to the accompanied decrease in solar absorbance. For a larger pitch of 1 μm, a proportionally larger decrease in particle size from 4R to R/4 is required to achieve a similar degree of temperature reduction by 8 ºC. (c) Increasing λ from 0.05 to 0.2 μm, temperature was reduced by 2.5 ºC due to the corresponding decrease in absorbance in the solar region.

To summarize the discussed simulation results, Table 1 below lists the designs presented and how certain parameters can be manipulated to control optical properties at specific wavelengths.

Table 1: Tunability of Optical Properties in Plain and Gold Particle-Coated Crumpled Graphene

Design	**Parameter Limit**	**Wavelength**	**Optical Modulation (Spectral Average)**
Biaxially-strained Randomly Crumpled Graphene on Cu	Characteristic length: 0.25 – 1.50 μm RMS amplitude: 0.25 – 1.50 μm	0.2 – 2 μm	Reflectivity: 0.19 – 0.78 Absorbance: 0.18 – 0.75
Biaxially-strained Randomly Crumpled Graphene on Cu	Thickness: 0.35 – 35 nm	0.2 – 2 μm	Reflectivity: 0.51 – 0.66 Absorbance: 0.31 – 0.45
Au Particle-coated Periodically Crumpled Graphene	Pitch: 0.14 – 1 μm Amplitude: 0.025 – 0.2 μm	0.05 – 1 μm	Reflectivity: 0 – 0.05 Transmittance: 0.55 – 0.74 Absorbance: 0 – 0.14
Au Particle-coated Periodically Crumpled Graphene	Particle radius: 8.375 – 33.5 nm (P = 0.4 μm), 4.1875 – 67 nm (P = 1 μm)	0.05 – 1 μm	For P = 0.4 μm: Reflectivity: 0 – 0.06 Transmittance: 0.55 – 0.74 Absorbance: 0 – 0.14 For P = 1 μm: Reflectivity: 0 – 0.09 Transmittance: 0.49 – 0.74 Absorbance: 0 – 0.15
Au Particle-coated Periodically Crumpled Graphene	Particle separation: 0.05 – 0.2 μm	0.05 – 1 μm	Reflectivity: 0 – 0.01 Transmittance: 0.67 – 0.73 Absorbance: 0.01 – 0.06

CHAPTER 4

DISCUSSION

It would be beneficial to continue the current analysis on the various parameters discussed as well as additional parameters one has not previously considered. Presently, the role of non-uniform particle distribution and radius is being explored, since this nonuniformity has demonstrated higher modulation of optical properties in previous designs. The effect of hierarchy on gold particle-coated crumpled graphene is also being investigated. Future effort will focus on the integration of multiple designs into a single, integrated system to achieve multifunctionality. One could envision a design which combines periodically and hierarchically crumpled graphene sheets with modifications such as embedded particles or surface textures. The successful integration of different graphene-based designs would not only lead to a better theoretical and experimental understanding of interlayer behavior, but also guide the development of adaptive, versatile, and lightweight composites for advanced thermal management applications.

CHAPTER 5

CONCLUSION

This thesis begins to address the knowledge gap which exists in current literature regarding fundamental mechanisms behind the dynamic optical properties of graphene by characterizing biaxially-strained randomly crumpled graphene and gold particle-coated periodically crumpled graphene through rigorous coupled-wave analysis (RCWA) and finite-difference time-domain (FDTD) computations. The results show a general increase in solar absorbance when photonic interaction, internal reflection, and diffraction between adjacent peaks are enhanced by increasing the aspect ratio and thickness within plain hierarchically crumpled graphene. For gold particle-coated periodically crumpled graphene, the presence of reflective particles at the surface induces electric field confinement, which becomes the dominant mechanism behind changes in absorbance within the UV-NIR region. Changes which increase the presence of gold particles, either by enlarging their size or decreasing the distance between them, will considerably improve confinement of electric field and thus solar absorbance. In the MIR region, changes in optical properties mainly consists of shifts in wavelength, offering broadband response which enables wavelength-specific applications. Thermal analysis using MATLAB shows a modest reduction in sample temperature with decreasing solar absorbance, identifying potential designs for graphene-based subambient cooling solutions.

References

[1] Ajay Rakkesh, R., Durgalakshmi, D., Karthe, P., & Balakumar, S. (2020). Anisotropic growth and strain-induced tunable optical properties of Ag–ZnO hierarchical nanostructures by a microwave synthesis method. *Materials Chemistry and Physics*. https://doi.org/10.1016/j.matchemphys.2020.122720

[2] Amorim, B., Cortijo, A., De Juan, F., Grushin, A. G., Guinea, F., Gutiérrez-Rubio, A., Ochoa, H., Parente, V., Roldán, R., San-Jose, P., Schiefele, J., Sturla, M., & Vozmediano, M. A. H. (2015). Novel effects of strains in graphene and other two dimensional materials. In *Physics Reports*. https://doi.org/10.1016/j.physrep.2015.12.006

[3] Bu, I. Y. Y. (2013). Highly conductive and transparent reduced graphene oxide/aluminium doped zinc oxide nanocomposite for the next generation solar cell applications. *Optical Materials*. https://doi.org/10.1016/j.optmat.2013.09.012

[4] Cao, Y., Zhu, J., Xu, J., & He, J. (2014). Tunable near-infrared photovoltaic and photoconductive properties of reduced graphene oxide thin films by controlling the number of reduced graphene oxide bilayers. *Carbon*. https://doi.org/10.1016/j.carbon.2014.06.029

[5] Chen, P. Y., Sodhi, J., Qiu, Y., Valentin, T. M., Steinberg, R. S., Wang, Z., Hurt, R. H., & Wong, I. Y. (2016). Multiscale Graphene Topographies Programmed by Sequential Mechanical Deformation. *Advanced Materials*. https://doi.org/10.1002/adma.201506194

[6] Chen, W., Gui, X., Yang, L., Zhu, H., & Tang, Z. (2019). Wrinkling of two-dimensional materials: Methods, properties and applications. In *Nanoscale Horizons*. https://doi.org/10.1039/c8nh00112j

[7] Guo, Y., Wang, T., Chen, F., Sun, X., Li, X., Yu, Z., Wan, P., & Chen, X. (2016). Hierarchical graphene-polyaniline nanocomposite films for high-performance flexible electronic gas sensors. *Nanoscale*. https://doi.org/10.1039/c6nr02540d

[8] Han, F., Yang, S., Jing, W., Jiang, K., Jiang, Z., Liu, H., & Li, L. (2014). A highly efficient synthetic process of graphene films with tunable optical properties. *Applied Surface Science*. https://doi.org/10.1016/j.apsusc.2014.05.222

[9] Hong, T. K., Lee, D. W., Choi, H. J., Shin, H. S., & Kim, B. S. (2010). Transparent, flexible conducting hybrid multilayer thin films of multiwalled carbon nanotubes with graphene nanosheets. *ACS Nano*. https://doi.org/10.1021/nn100897g

[10] Kang, J., Lim, T., Jeong, M. H., & Suk, J. W. (2019). Graphene papers with tailored pore

structures fabricated from crumpled graphene spheres. *Nanomaterials*. https://doi.org/10.3390/nano9060815

[11] Kang, P., Kim, K. H., Park, H. G., & Nam, S. W. (2018). Crumple nanostructured graphene for mechanically reconfigurable plasmonic resonances. *Optics InfoBase Conference Papers*. https://doi.org/10.1364/FIO.2018.JW3A.44

[12] Kang, P., Kim, K. H., Park, H. G., & Nam, S. W. (2018). Mechanically reconfigurable architectured graphene for tunable plasmonic resonances. *Light: Science and Applications*. https://doi.org/10.1038/s41377-018-0002-4

[13] Khattak, M. I., Ullah, Z., Al-Hasan, M., & Sheikh, F. (2020). Enhanced tunable plasmonic resonance in crumpled graphene resonators loaded with gate tunable metamaterials. *Optics Express*. https://doi.org/10.1364/oe.411014

[14] Krishna, A., Kim, J. M., Leem, J., Wang, M. C., Nam, S., & Lee, J. (2019). Ultraviolet to Mid-Infrared Emissivity Control by Mechanically Reconfigurable Graphene. *Nano Letters*. https://doi.org/10.1021/acs.nanolett.9b01358

[15] Lee, B., Lee, C., Liu, T., Eom, K., Chen, Z., Noda, S., Fuller, T. F., Jang, H. D., & Lee, S. W. (2016). Hierarchical networks of redox-active reduced crumpled graphene oxide and functionalized few-walled carbon nanotubes for rapid electrochemical energy storage. *Nanoscale*. https://doi.org/10.1039/c6nr02013e

[16] Lee, D. W., Hong, T. K., Kang, D., Lee, J., Heo, M., Kim, J. Y., Kim, B. S., & Shin, H. S. (2011). Highly controllable transparent and conducting thin films using layer-by-layer assembly of oppositely charged reduced graphene oxides. *Journal of Materials Chemistry*. https://doi.org/10.1039/c0jm02270e

[17] Leem, J., Wang, M. C., Kang, P., & Nam, S. (2015). Mechanically Self-Assembled, Three-Dimensional Graphene-Gold Hybrid Nanostructures for Advanced Nanoplasmonic Sensors. *Nano Letters*. https://doi.org/10.1021/acs.nanolett.5b03672

[18] Li, K., Chang, T. H., Li, Z., Yang, H., Fu, F., Li, T., Ho, J. S., & Chen, P. Y. (2019). Biomimetic MXene Textures with Enhanced Light-to-Heat Conversion for Solar Steam Generation and Wearable Thermal Management. *Advanced Energy Materials*. https://doi.org/10.1002/aenm.201901687

[19] Li, Z., Zhai, Y., Wang, Y., Wendland, G. M., Yin, X., & Xiao, J. (2017). Harnessing Surface Wrinkling–Cracking Patterns for Tunable Optical Transmittance. *Advanced Optical*

Materials. https://doi.org/10.1002/adom.201700425

[20] Liu, L., Niu, Z., Zhang, L., Zhou, W., Chen, X., & Xie, S. (2014). Nanostructured graphene composite papers for highly flexible and foldable supercapacitors. *Advanced Materials*. https://doi.org/10.1002/adma.201401513

[21] Liu, T., Kim, D., Han, H., Mohd Yusoff, A. R. Bin, & Jang, J. (2015). Fine-tuning optical and electronic properties of graphene oxide for highly efficient perovskite solar cells. *Nanoscale*. https://doi.org/10.1039/c5nr01433f

[22] Liu, Y., & Zhang, D. (2017). Synergetic effect in the multifunctional composite film of graphene-TiO2with transparent conductive, photocatalytic and strain sensing properties. *Journal of Alloys and Compounds*. https://doi.org/10.1016/j.jallcom.2016.11.366

[23] Luo, B., Chen, B., Meng, L., Geng, D., Liu, H., Xu, J., Zhang, Z., Zhang, H., Peng, L., He, L., Hu, W., Liu, Y., & Yu, G. (2014). Layer-stacking growth and electrical transport of hierarchical graphene architectures. *Advanced Materials*. https://doi.org/10.1002/adma.201305627

[24] Luo, J., Zhao, X., Wu, J., Jang, H. D., Kung, H. H., & Huang, J. (2012). Crumpled graphene-encapsulated Si nanoparticles for lithium ion battery anodes. *Journal of Physical Chemistry Letters*. https://doi.org/10.1021/jz3006892

[25] Maity, N., Mandal, A., & Nandi, A. K. (2016). Hierarchical nanostructured polyaniline functionalized graphene/poly(vinylidene fluoride) composites for improved dielectric performances. *Polymer*. https://doi.org/10.1016/j.polymer.2016.09.048

[26] Mu, J., Hou, C., Wang, G., Wang, X., Zhang, Q., Li, Y., Wang, H., & Zhu, M. (2016). An Elastic Transparent Conductor Based on Hierarchically Wrinkled Reduced Graphene Oxide for Artificial Muscles and Sensors. *Advanced Materials*. https://doi.org/10.1002/adma.201603395

[27] Nguyen Bich, H., & Nguyen Van, H. (2016). Promising applications of graphene and graphene-based nanostructures. In *Advances in Natural Sciences: Nanoscience and Nanotechnology*. https://doi.org/10.1088/2043-6262/7/2/023002

[28] Nguyen, D. D., Tai, N. H., Chen, S. Y., & Chueh, Y. L. (2012). Controlled growth of carbon nanotube-graphene hybrid materials for flexible and transparent conductors and electron field emitters. *Nanoscale*. https://doi.org/10.1039/c1nr11328c

[29] Ong, H. Y., Shrestha, M., & Lau, G. K. (2015). Microscopically crumpled indium-tin-

oxide thin films as compliant electrodes with tunable transmittance. *Applied Physics Letters*. https://doi.org/10.1063/1.4932115

[30] Shi, H. F., Wang, C., Sun, Z. P., Zhou, Y. L., Jin, K. J., & Yang, G. Z. (2014). Transparent conductive reduced graphene oxide thin films produced by spray coating. *Science China: Physics, Mechanics and Astronomy*. https://doi.org/10.1007/s11433-014-5614-y

[31] Su, B. L., Sanchez, C., & Yang, X. Y. (2011). Hierarchically Structured Porous Materials: From Nanoscience to Catalysis, Separation, Optics, Energy, and Life Science. In *Hierarchically Structured Porous Materials: From Nanoscience to Catalysis, Separation, Optics, Energy, and Life Science*. https://doi.org/10.1002/9783527639588

[32] Sun, M. H., Huang, S. Z., Chen, L. H., Li, Y., Yang, X. Y., Yuan, Z. Y., & Su, B. L. (2016). Applications of hierarchically structured porous materials from energy storage and conversion, catalysis, photocatalysis, adsorption, separation, and sensing to biomedicine. *Chemical Society Reviews*. https://doi.org/10.1039/c6cs00135a

[33] Takatani, T., Mukaigawa, Y., Matsushita, Y., & Yagi, Y. (2018). Decomposition of reflection and scattering by multiple-weighted measurements. *IPSJ Transactions on Computer Vision and Applications*. https://doi.org/10.1186/s41074-018-0049-4

[34] Thomas, A. V., Andow, B. C., Suresh, S., Eksik, O., Yin, J., Dyson, A. H., & Koratkar, N. (2015). Controlled crumpling of graphene oxide films for tunable optical transmittance. *Advanced Materials*. https://doi.org/10.1002/adma.201405821

[35] Wan, J., Xu, Y., Ozdemir, B., Xu, L., Sushkov, A. B., Yang, Z., Yang, B., Drew, D., Barone, V., & Hu, L. (2017). Tunable Broadband Nanocarbon Transparent Conductor by Electrochemical Intercalation. *ACS Nano*. https://doi.org/10.1021/acsnano.6b07191

[36] Wang, G. F., Qin, H., Gao, X., Cao, Y., Wang, W., Wang, F. C., Wu, H. A., Cong, H. P., & Yu, S. H. (2018). Graphene Thin Films by Noncovalent-Interaction-Driven Assembly of Graphene Monolayers for Flexible Supercapacitors. *Chem*. https://doi.org/10.1016/j.chempr.2018.01.008

[37] Wang, L., Ye, Y., Lu, X., Wen, Z., Li, Z., Hou, H., & Song, Y. (2013). Hierarchical nanocomposites of polyaniline nanowire arrays on reduced graphene oxide sheets for supercapacitors. *Scientific Reports*. https://doi.org/10.1038/srep03568

[38] Yang, X. Y., Chen, L. H., Li, Y., Rooke, J. C., Sanchez, C., & Su, B. L. (2017). Hierarchically porous materials: Synthesis strategies and structure design. In *Chemical Society*

Reviews. https://doi.org/10.1039/c6cs00829a

[39] Yuan, J., Ma, L. P., Pei, S., Du, J., Su, Y., Ren, W., & Cheng, H. M. (2013). Tuning the electrical and optical properties of graphene by ozone treatment for patterning monolithic transparent electrodes. *ACS Nano*. https://doi.org/10.1021/nn400682u

[40] Yun, J. M., Jung, C. H., Noh, Y. J., Jeon, Y. J., Kim, S. S., Kim, D. Y., & Na, S. I. (2015). Morphological, optical, and electrical investigations of solution-processed reduced graphene oxide and its application to transparent electrodes in organic solar cells. *Journal of Industrial and Engineering Chemistry*. https://doi.org/10.1016/j.jiec.2014.04.026

[41] Yun, Y. S., Park, Y. U., Chang, S. J., Kim, B. H., Choi, J., Wang, J., Zhang, D., Braun, P. V., Jin, H. J., & Kang, K. (2016). Crumpled graphene paper for high power sodium battery anode. *Carbon*. https://doi.org/10.1016/j.carbon.2015.12.047

[42] Zang, J., Cao, C., Feng, Y., Liu, J., & Zhao, X. (2014). Stretchable and High-Performance Supercapacitors with Crumpled Graphene Papers. *Scientific Reports*. https://doi.org/10.1038/srep06492

[43] Zang, J., Ryu, S., Pugno, N., Wang, Q., Tu, Q., Buehler, M. J., & Zhao, X. (2013). Multifunctionality and control of the crumpling and unfolding of large-area graphene. *Nature Materials*. https://doi.org/10.1038/nmat3542

[44] Zhu, Y., Cai, W., Piner, R. D., Velamakanni, A., & Ruoff, R. S. (2009). Transparent self-assembled films of reduced graphene oxide platelets. *Applied Physics Letters*. https://doi.org/10.1063/1.3212862

APPENDIX A

SUPPLEMENTARY

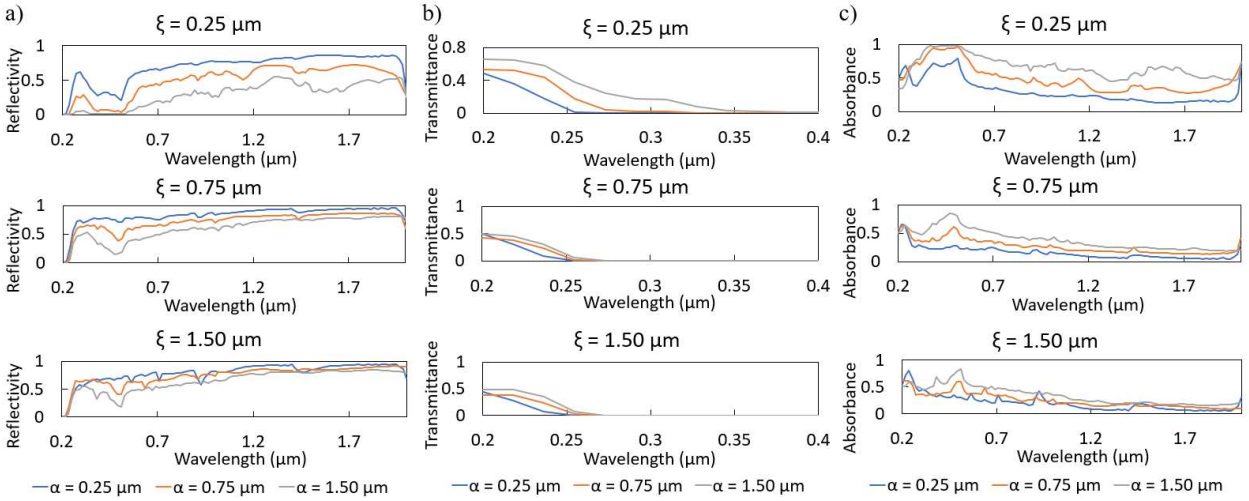

Figure S1: (a-c) Reflectivity, transmittance, and absorbance of biaxially-strained randomly crumpled graphene in the near-infrared region with varying correlation lengths (ξ = 0.25, 0.75, 1.50 μm) and RMS amplitudes (α = 0.25, 0.75, 1.50 μm) obtained through FDTD simulations. (a) As α decreases and ξ increases, surface roughness is reduced, and reflectivity increases due to the enhancement in specular reflection. (b) Simultaneously, one observes a minor decrease in transmittance between 0.2 and 0.25 μm. Beyond 0.25 μm, transmittance drops to zero when ξ exceeds 0.75 μm. (c) Absorbance is reduced and is attributed the reduction in internal scattering with decreased surface roughness.

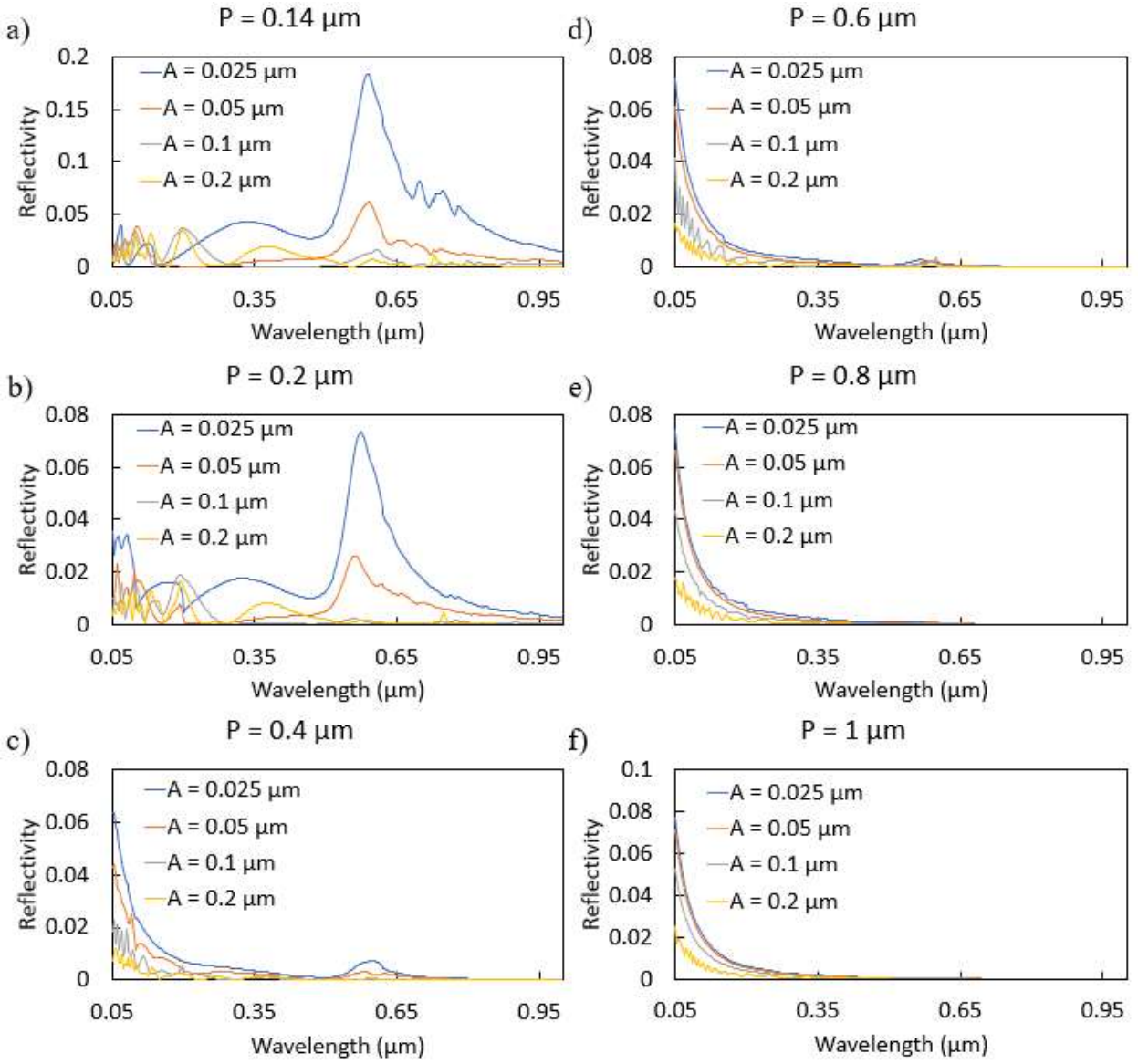

Figure S2: (a-f) Reflectivity of gold particle-coated periodically crumpled graphene in the near-infrared region with varying amplitudes (A = 0.025, 0.05, 0.1, 0.2 µm) for six fixed pitch values (P = 0.14, 0.2, 0.4, 0.6, 0.8, 1 µm) obtained through FDTD simulations. Note that the modulation in reflectivity is more significant with smaller pitch values due to the larger change in aspect ratio when the amplitude is varied.

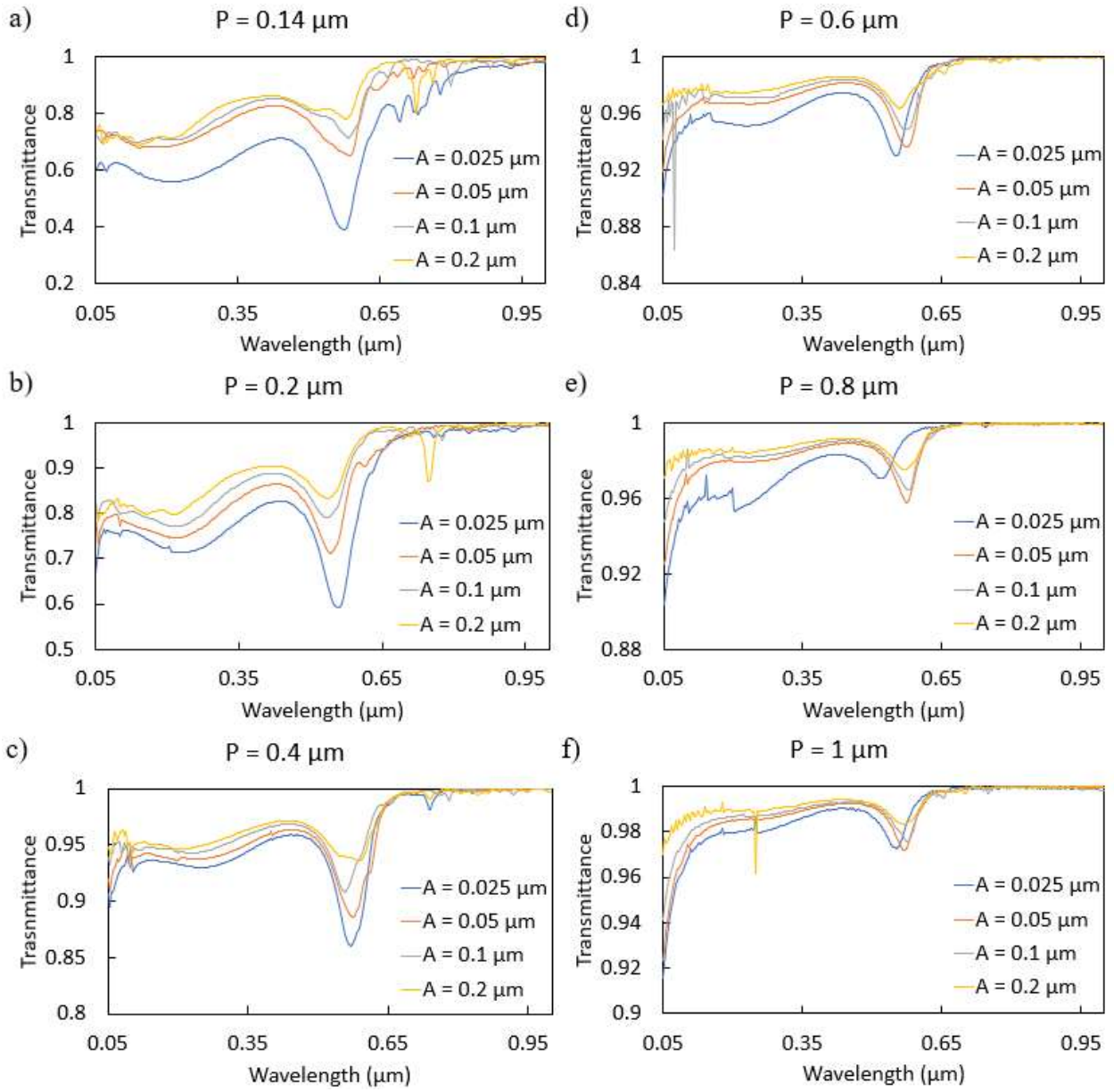

Figure S3: (a-f) Transmittance of gold particle-coated periodically crumpled graphene in the near-infrared region with varying amplitudes (A = 0.025, 0.05, 0.1, 0.2 µm) for six fixed pitch values (P = 0.14, 0.2, 0.4, 0.6, 0.8, 1 µm) obtained through FDTD simulations. Note that the modulation in transmittance is more significant with smaller pitch values due to the larger change in aspect ratio when the amplitude is varied.

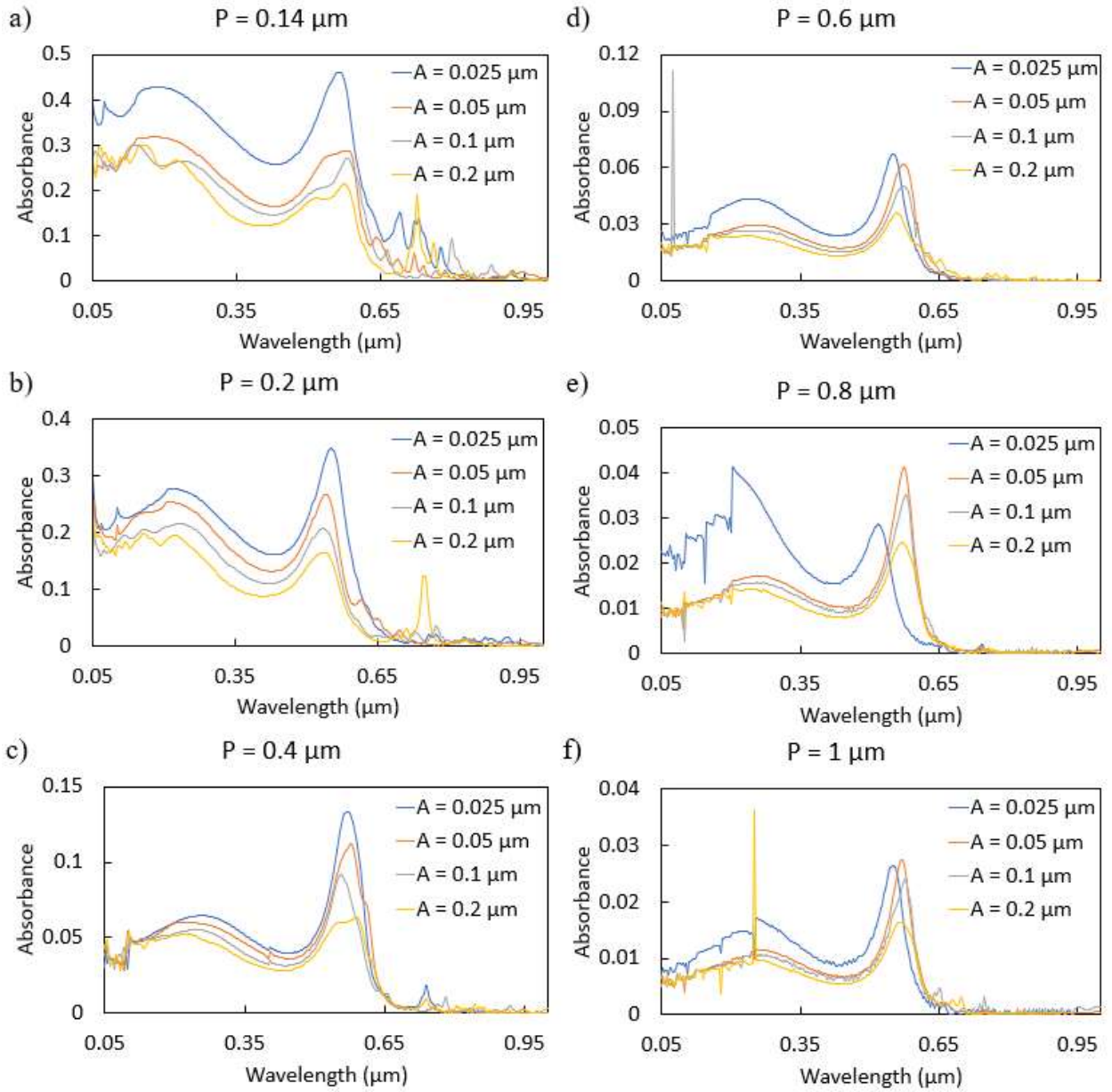

Figure S4: (a-f) Absorbance of gold particle-coated periodically crumpled graphene in the near-infrared region with varying amplitudes (A = 0.025, 0.05, 0.1, 0.2 µm) for six fixed pitch values (P = 0.14, 0.2, 0.4, 0.6, 0.8, 1 µm) obtained through FDTD simulations. Note that the modulation in absorbance is more significant with smaller pitch values due to the larger change in aspect ratio when the amplitude is varied.

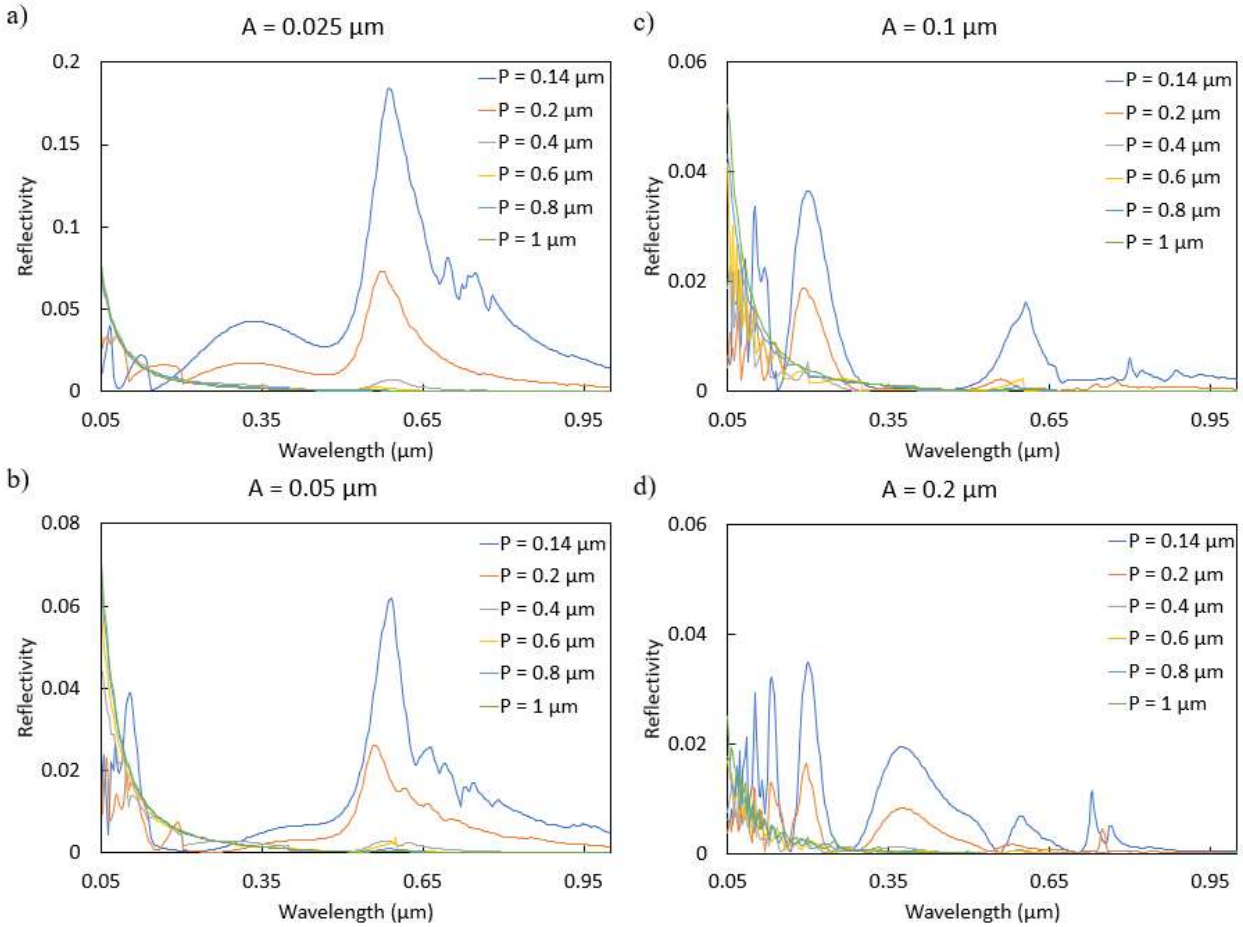

Figure S5: (a-d) Reflectivity of gold particle-coated periodically crumpled graphene in the near-infrared region with varying pitch values (P = 0.14, 0.2, 0.4, 0.6, 0.8, 1 µm) for four fixed amplitudes (A = 0.025, 0.05, 0.1, 0.2 µm) obtained through FDTD simulations. Note that the increase in reflectivity is more significant with smaller amplitude values due to innate limitations imposed by this structure.

.

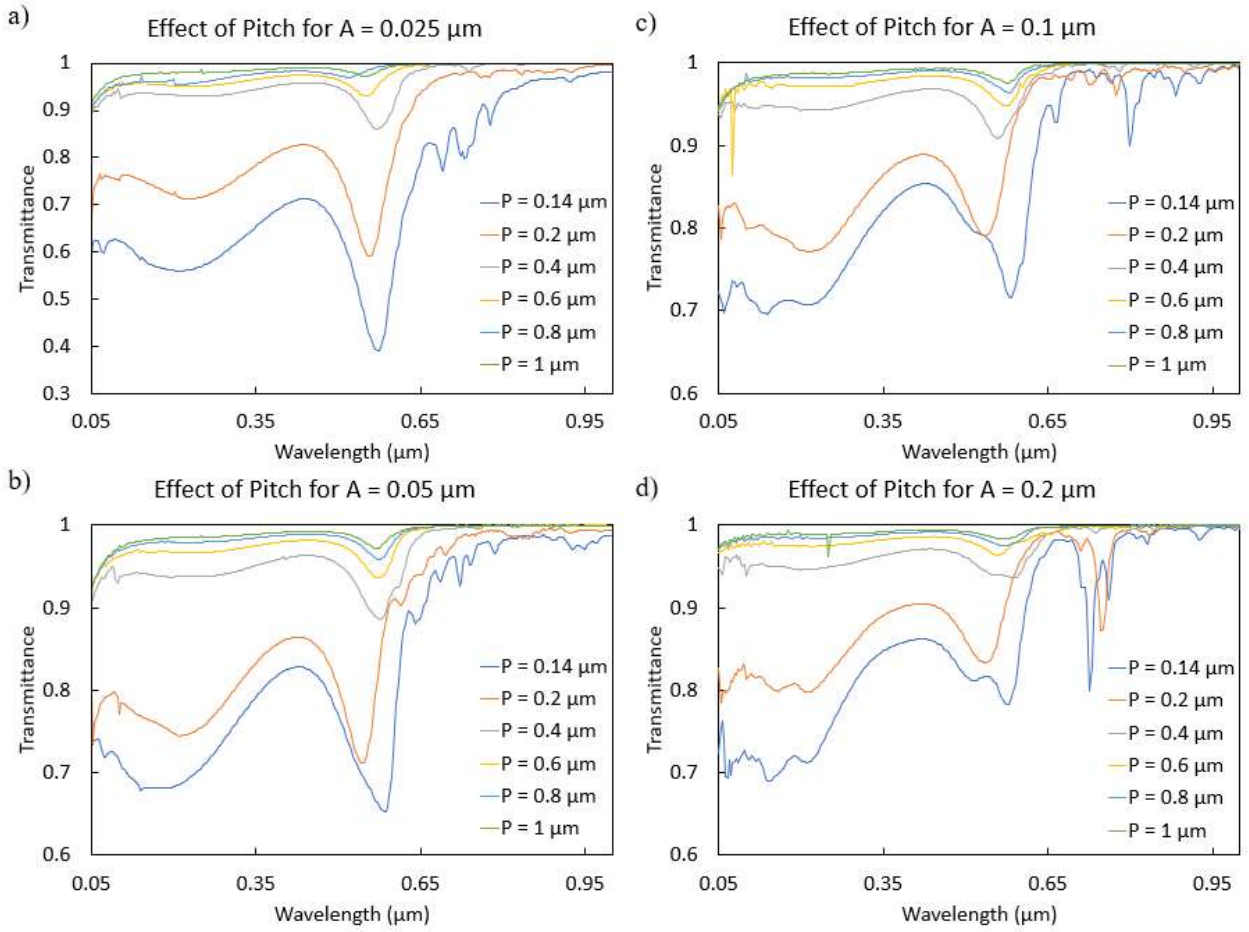

Figure S6: (a-d) Transmittance of gold particle-coated periodically crumpled graphene in the near-infrared region with varying pitch values (P = 0.14, 0.2, 0.4, 0.6, 0.8, 1 µm) for four fixed amplitudes (A = 0.025, 0.05, 0.1, 0.2 µm) obtained through FDTD simulations. Note that the increase in transmittance is more significant with smaller amplitude values due to innate limitations imposed by this structure.

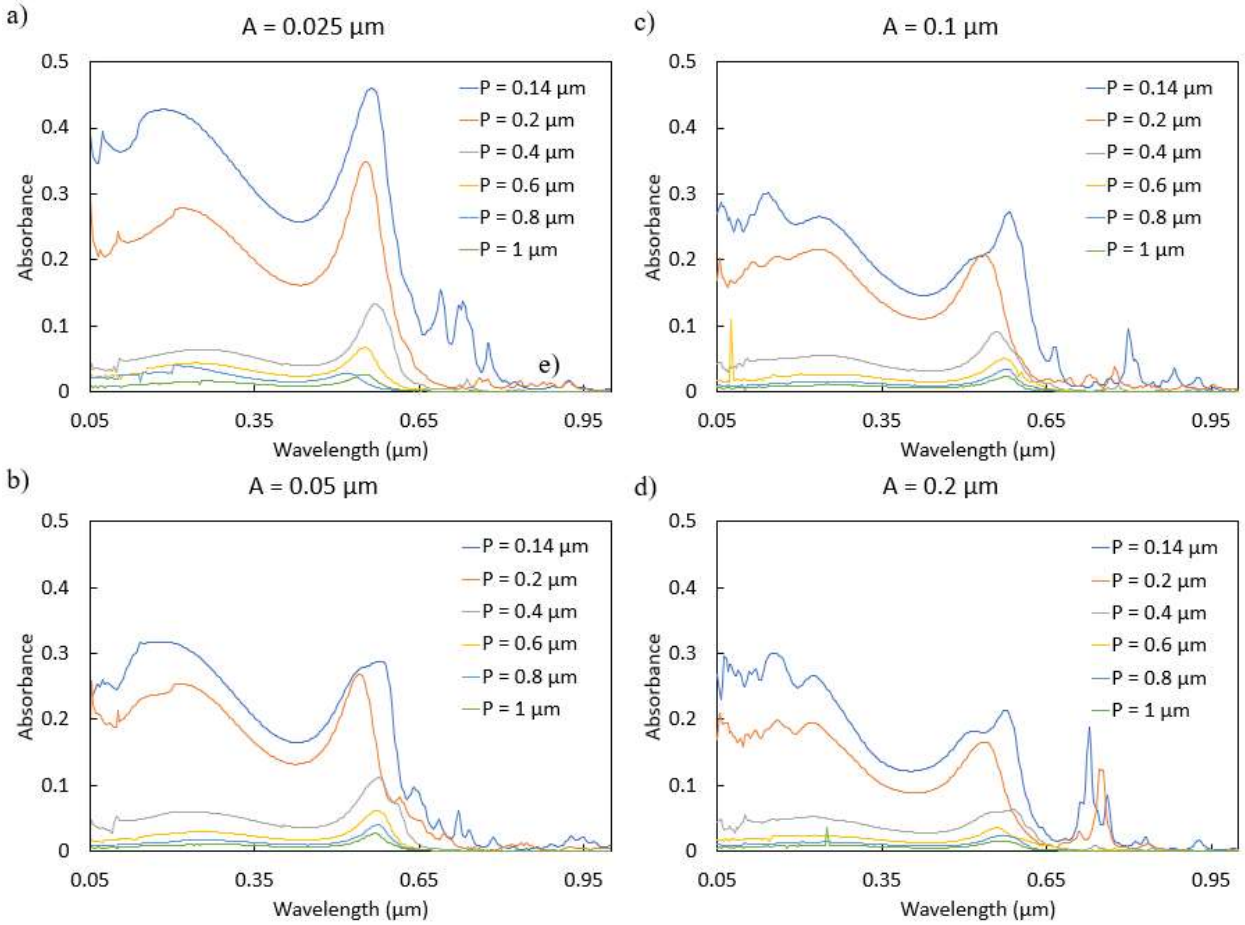

Figure S7: (a-d) Absorbance of gold particle-coated periodically crumpled graphene in the near-infrared region with varying pitch values (P = 0.14, 0.2, 0.4, 0.6, 0.8, 1 µm) for four fixed amplitudes (A = 0.025, 0.05, 0.1, 0.2 µm) obtained through FDTD simulations. Note that the increase in absorbance is more significant with smaller amplitude values due to innate limitations imposed by this structure.

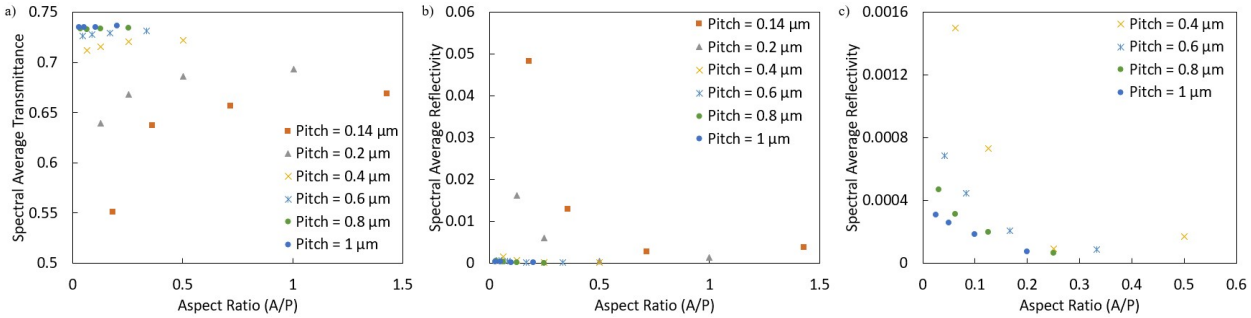

Figure S8: (a-c) Spectral average transmittance and reflectivity of gold particle-coated periodically crumpled graphene in the ultraviolet-near-infrared (UV-NIR, 0.05–1 µm) region as a function of aspect ratio for six different fixed pitch values (P = 0.14, 0.2, 0.4, 0.6, 0.8, 1 µm). The various points of the same color correspond to changing amplitudes (A = 0.025, 0.05, 0.1, 0.2 µm). (a) Average transmittance is reduced from 0.74 to 0.55 by minimizing A and P due to the diminished exposure of underlying transmissive graphene. It can be noted that the increase in transmittance is more significant with smaller pitch values due to the larger change in aspect ratio when the amplitude is varied. For a pitch of 0.14 µm, the spectral average transmittance decreased by 0.118, compared to 0.001 for a pitch of 1 µm, when A decreased from 0.2 to 0.025 µm. (b) Average reflectivity is marginally improved by as much as 0.05 with decreasing A and P due to the closer proximity of gold particles. It can be noted that the increase in reflectivity is more significant with smaller pitch values due to the larger change in aspect ratio when the amplitude is varied. For a pitch of 0.14 µm, the spectral average reflectivity increased by 0.045, compared to 0.0002 for a pitch of 1 µm, when A decreased from 0.2 to 0.025 µm. (c) Inset plot of (b) showing cases with P equal to or larger than 0.4 µm.

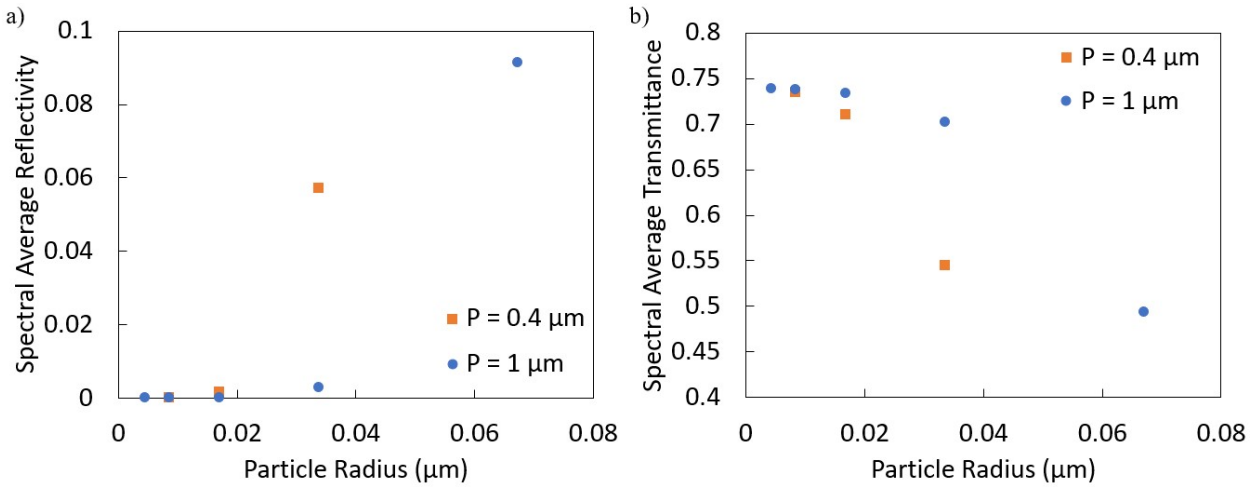

Figure S9: (a,b) Spectral average reflectivity and transmittance of gold particle-coated periodically crumpled graphene in the ultraviolet-near-infrared (UV-NIR, 0.05–1 µm) region as a function of particle radius for the two different pitch values (P = 0.4, 1 µm) obtained through FDTD simulations. (a) For a pitch of 0.4 µm, as r was lowered from 33.5 (2R) to 8.375 nm (R/2), average reflectivity decreased from 0.06 to effectively zero. For a pitch of 1 µm, as r was lowered from 67 (4R) to 4.1875 nm (R/4), average reflectivity decreased from 0.09 to zero. The reduction in reflectivity with smaller r is due to the decreased presence of reflective gold particles. (b) For a pitch of 0.4 µm, as r was lowered 2R to R/2, average transmittance increased from 0.55 to 0.74. For a pitch of 1 µm, as r was lowered from 4R to R/4, average transmittance increased from 0.49 to 0.74. The improve in transmittance with smaller r is due to the increased exposure of underlying transmissive graphene.

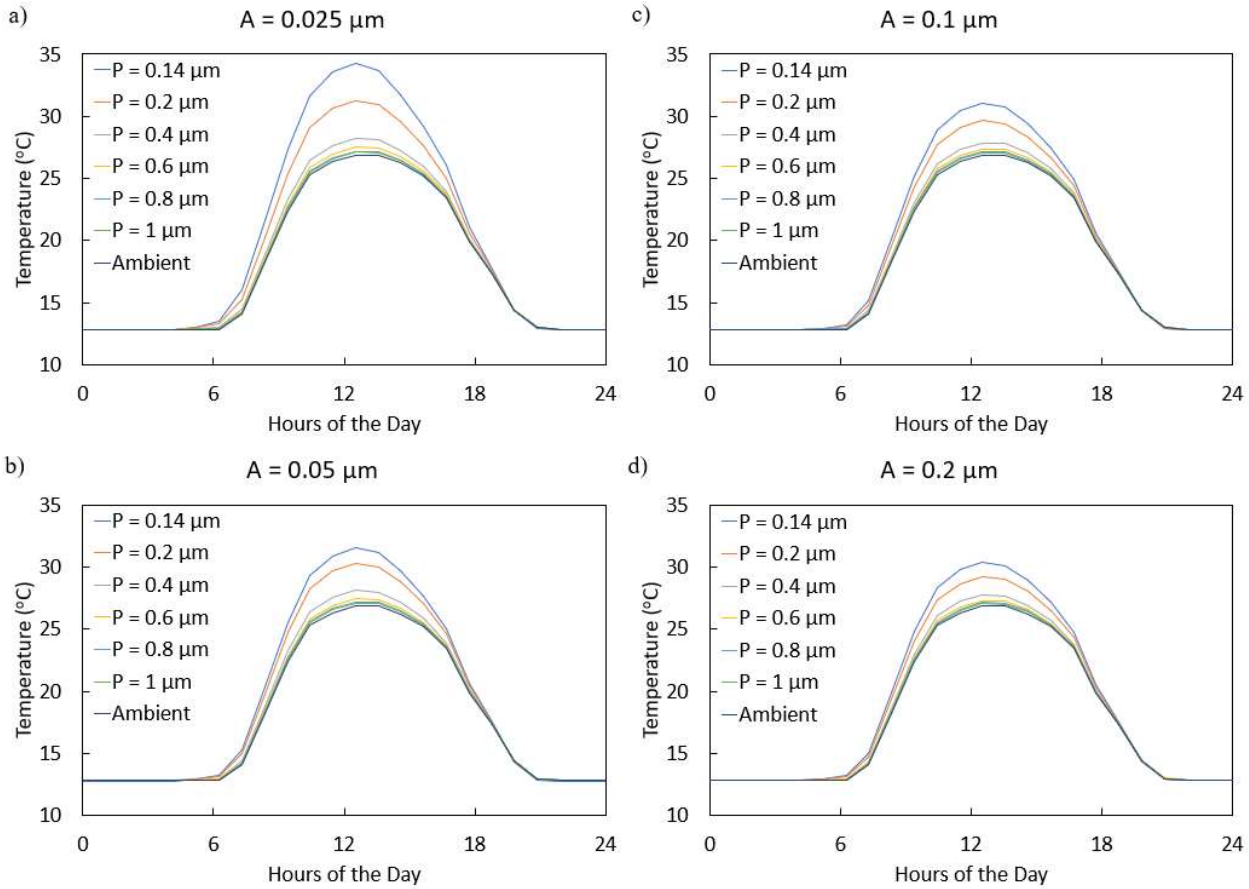

Figure S10: (a-d) Effect of pitch (P) on radiative cooling performance of gold particle-coated periodically crumpled graphene for four fixed amplitudes (A = 0.025, 0.05, 0.1, 0.2 µm) obtained through MATLAB. With an amplitude of 0.025 µm, increasing the pitch from 0.14 to 1 µm reduced the daytime temperature by 7.1 °C. It can be noted that the temperature reduction is more significant with smaller amplitudes. When the pitch exceeds 0.8 µm, near-ambient cooling was achieved during the day under the specified simulation conditions.

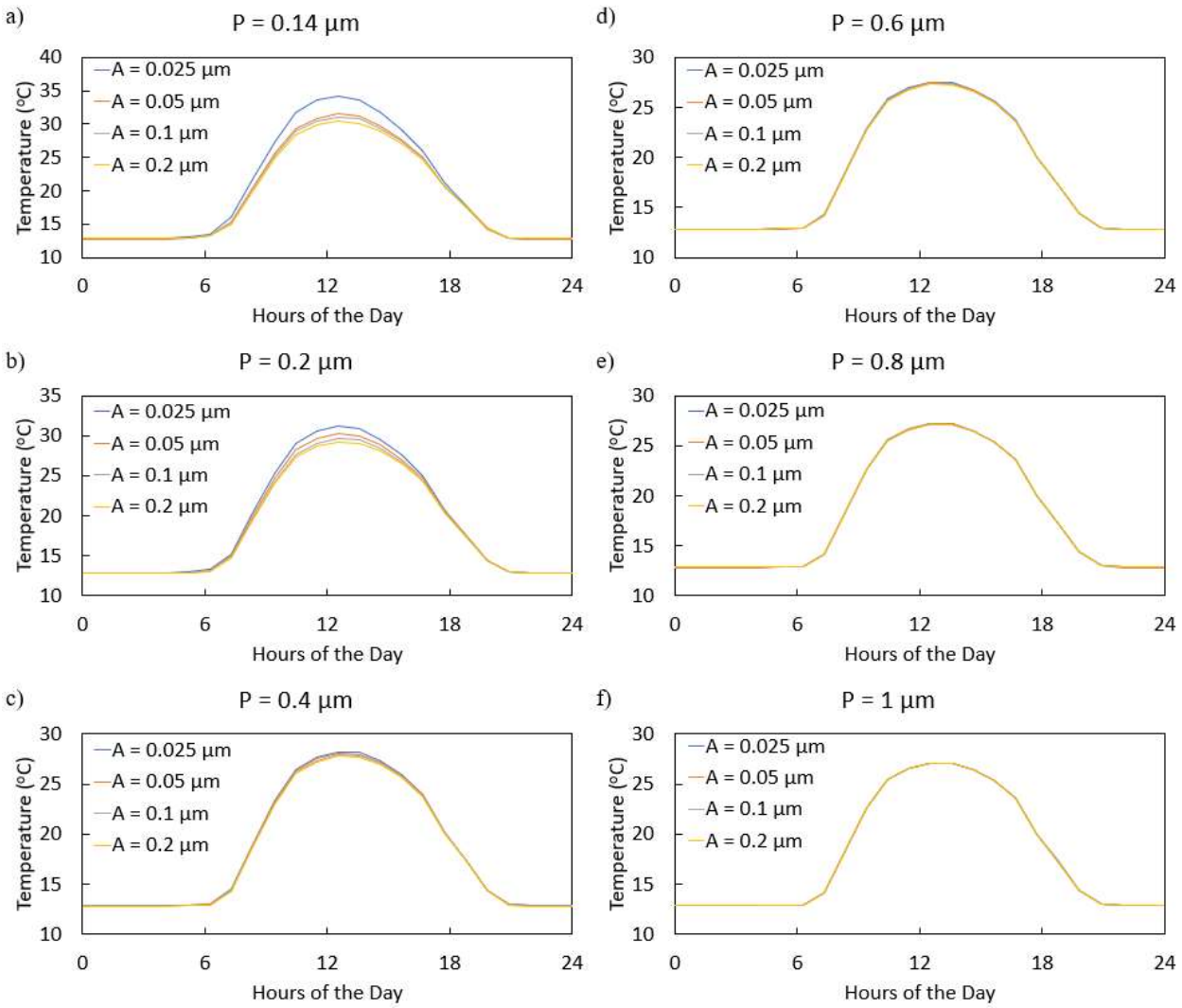

Figure S11: (a-f) Effect of amplitude (A) on radiative cooling performance of gold particle-coated periodically crumpled graphene for six fixed pitch values (P = 0.14, 0.2, 0.4, 0.6, 0.8, 1 µm) obtained through MATLAB. With a pitch of 0.14 µm, increasing the amplitude from 0.025 to 0.2 µm reduced the daytime temperature by 3.9 °C. It can be noted that the temperature reduction is more significant with smaller pitch values due to the larger change in solar absorbance and becomes marginal when the pitch exceeds 0.4 µm.